1. Report No.	2. Government Accession No.	3. Recipient's Catalog No.
ICAR/401131		

4. Title and Subtitle	5. Report Date
ACCEPTABILITY CRITERIA FOR HIGH FINES CONTENT AGGREGATE PAVEMENT LAYERS	12-31-2007
	6. Performing Organization Code
7. Author(s)	8. Performing Organization Report No.
Reza Salehi Ashtiani and Dallas Little, Ph.D.	
9. Performing Organization Name and Address	10. Work Unit No. (TRAIS)
Texas Transportation Institute The Texas A&M University System College Station, Texas 77843-3135	11. Contracts or Grant No. Project No. ICAR/401131
1. Sponsoring Agency Name and Address	13. Type of Report and Period Covered
INTERNATIONAL CENTER FOR AGGREGATES RESEARCH (ICAR)	14. Sponsoring Agency Code

15. Supplementary Notes

16. Abstract

The objective of this study was to evaluate the impact of increasing fines content on the performance of unbound (unstabilized) and lightly stabilized aggregate systems. The aggregate systems analyzed varied in the amount of mineral fines, the moisture state during curing and at the time of testing, and the amount of Portland cement used to stabilize the blend. The evaluation was based on measurements of anisotropic resilient properties, permanent deformation, and unconfined compressive strengths of aggregate systems. In addition, the nonlinear anisotropic resilient properties of the aggregate blends were used in a finite element program to determine critical pavement responses. Aggregate systems with higher fines contents were, as expected, more sensitive to moisture than control systems with standard fines contents. The increase in the fines content in the unbound systems when molding moisture was greater than optimum dramatically diminished the quality of performance. However, the aggregate systems with higher fines benefited considerably from low percentages of cement stabilizer. Researchers found that with the proper design of fines content, cement content, and moisture, the performance of the stabilized systems with high fines content can perform equivalent to or even better than systems with standard fines content. This was clearly demonstrated that by enhancing the resilient properties (an increase in stiffness and a decrease in the level of anisotropy), permanent deformation of the aggregate systems were significantly reduced. This finding was in conformity with unconfined compressive strength of lightly stabilized high fine systems.

17. Key Words	18. Distribution Statement
Aggregate, Fines, Anisotropy, Unbound Granular Base, Stabilized Aggregate Base, Stabilization, Aggregate Base, Resilient Modulus, Cross-anisotropy	No restrictions. This document is available to the public through the National Technical Information Service Springfield, Virginia 22161.

19. Security Classification of this report	20. Security Classification (of this page)	21. No. of Pages	22. Price
Unclassified	Unclassified	100	

ACCEPTABILITY CRITERIA FOR HIGH FINES CONTENT AGGREGATE PAVEMENT LAYERS

by

Reza Salehi Ashtiani
Graduate Research Assistant
Texas A&M University
and

Dallas N. Little, Ph.D.
Senior Research Fellow
Texas A&M University

Report No. ICAR/401131

Sponsored by the
International Center for Aggregates Research (ICAR)

TEXAS TRANSPORTATION INSTITUTE
The Texas A&M University System
College Station, Texas 77845

TABLE OF CONTENTS

LIST OF FIGURES vii

LIST OF TABLES x

CHAPTER 1: **LITERATURE REVIEW OF FINES** 1

1.1 Background 1

1.2 Definition of Fines 1

1.3 Types and Amounts Produced 2

1.4 Civil Engineering Applications of Waste or Byproduct Fines, Review of Literature 4

1.5 Impact of Lithology on Fines Generation 6

1.6 Impact of Crusher Type in Fines Generation 8

1.7 Issues with the Crushers 8

CHAPTER 2: LABORATORY TESTS AND MATERIALS 11

2.1 Materials and Experimental Variables 11

2.2 Material Tests 11

2.3 Specimen Conditioning 13

2.4 Laboratory Tests for Mechanical Behavior of Aggregates 15

2.5 Testing Protocol 17

2.6 Compression Regime 18

2.7 Shear Regime 18

2.8 Extension Regime 19

2.9 Permanent Deformation Potential 21

2.10 Unconfined Compressive Strength Properties 21

CHAPTER 3: LABORATORY TEST RESULTS AND ANALYSIS 23

3.1 Materials Tested 23

3.2 Volumetric Relations 23

3.3 Resilient Properties 29

3.4 Analysis of Modular Ratios 30

CHAPTER 4: TEST RESULTS AND ANALYSIS OF PAVEMENT STRUCTURE 33
4.1 Permanent Deformation Test Results 33
4.2 Unconfined Compressive Strength 34
4.3 Fines under Light Microscope 38
4.4 Finite Element Analysis 43
CHAPTER 5: PERFORMANCE PREDICTION OF AGGREGATE BASES 47
5.1 Degree of Nonlinearity 47
5.2 Measures of Nonlinearity 49
5.3 Analysis of the Degree of Nonlinearity 51
5.4 Structural Stability of the Aggregate Systems 54
5.5 Analysis of Shear Stresses in the Base Layer 56
5.6 Analysis of Shear Strength Ratios 59
5.7 Plastic Deformation at the Surface 61
REFERENCES 64
APPENDIX A: TABLE OF MATERIAL PROPERTIES 66
APPENDIX B: **TABLE OF MODULAR RATIOS** 75

TABLE OF FIGURES

Figure 1-1 Impact of Lithology on Fines Generation Based on Weight.....7
Figure 1-2 Impact of Lithology on Fines Generation Based on Percentage.....7
Figure 2-2 Stress Path Induced by Moving Wheel on Pavement 15
Figure 2-3 RaTT Cell Assembly.....16
Figure 2-4 Stress Path for ICAR Test Protocol 20
Figure 3-1 Schematic Representation of Synergistic Interaction of Stabilizer, Moisture Content, and Fines Content 23
Figure 3-2 Dry Densities of Unstabilized Systems Compacted in Optimum and Wet of Optimum Moisture Conditions 26
Figure 3-3 Dry Densities of 1 Percent Cement Stabilized Systems Compacted in Optimum and Wet of Optimum Moisture Conditions 26
Figure 3-4 Dry Densities of 2 Percent Cement Stabilized Systems Compacted in Optimum and Wet of Optimum Moisture Conditions 27
Figure 3-5 Impact of the Variation of Fines Content and Stabilizer Content on the Dry Density of Aggregate Systems Molded at Optimum Moisture Content.....28
Figure 3-6 Impact of the Variation of Fines Content and Stabilizer Content on the Dry Density of Aggregate Systems Molded at Wet of Optimum Moisture Content.....29
Figure 3-7 Average Modular Ratio for Unbound Aggregate Systems 31
Figure 3-8 Average Modular Ratios for 1 Percent Cement Stabilized Aggregate Systems 32
Figure 3-9 Average Modular Ratios for 2 Percent Cement Stabilized Aggregate Systems 32
Figure 4-1 Comparison of Permanent Strain at Optimum Moisture Content.....33
Figure 4-2 Comparison of Permanent Strain at Wet of Optimum Moisture Content.....34
Figure 4-3 Unconfined Compressive Strength for Conditioned Aggregate Systems.....35
Figure 4-4 Shear Banding in 2 Percent Cement Stabilized High Fines System V3 36
Figure 4-5 Degradation of Particles for Coarse Gradation V1 under Wet Conditions.....37
Figure 4-6 Light Microscope Image of Granite Materials (A8) Smaller than 0.15 mm (Passing Sieve #100).....38
Figure 4-7 Light Microscope Image of Granite Materials (A8) Smaller than 0.075 mm (Passing Sieve #200).....39

Figure 4-8 Light Microscope Image of Siliceous Gravel (A5) Smaller than 0.15 mm (Passing Sieve #100)....39
Figure 4-9 Light Microscope Image of Siliceous Gravel (A5) Smaller than 0.075 mm (Passing Sieve #200)....40
Figure 4-10 Light Microscope Image of Siliceous Gravel (A6) Smaller than 0.15 mm (Passing Sieve #100)....40
Figure 4-11 Light Microscope Image of Siliceous Gravel (A6) Smaller than 0.075 mm (Passing Sieve #200)....41
Figure 4-12 Light Microscope Image of Limestone (A7) Smaller than 0.15 mm (Passing Sieve #100)....41
Figure 4-13 Light Microscope Image of Limestone (A7) Smaller than 0.075 mm (Passing Sieve #200)....42
Figure 4-14 Light Microscope Image of Limestone (A2) Smaller than 0.15 mm (Passing Sieve #100)....42
Figure 4-15 Light Microscope Image of Limestone (A2) Smaller than 0.075 mm (Passing Sieve #200)....43
Figure 4-16 Comparison of Vertical Strains at the Top of the Subgrade for a Pavement Structure with Different Aggregate Systems Tested under Wet Conditions....45
Figure 4-17 Comparison of Tensile Strains at the Bottom of the Asphalt for a Pavement Structure with Different Aggregate Systems Tested at Wet Conditions....46
Figure 5-1 Characteristic Stress-Strain Behavior of Soils....48
Figure 5-2 Strain Level and Prescribed Stress Protocols in the Lab....49
Figure 5-3 Typical Stress-Strain Behavior for Stiff and Soft Aggregate System....50
Figure 5-4 Variation of the Degree of Nonlinearity Based on Deviatoric Stress Ratios....52
Figure 5-5 Analysis of the Degree of Nonlinearity Based on Deviatoric Stress Ratios....53
Figure 5-6 Analysis of the Degree of Nonlinearity Based on Strain Ratios....53
Figure 5-7 Illustration of the Concept of the Shear Stress Ratio Using the Mohr Circle....54
Figure 5-8 Shear Stress Distribution in the Base Layer for Controlled System (V1)....56
Figure 5-9 Shear Stress Distributions in the Base Layer for Unstabilized (V3) System under Wet Conditions....57
Figure 5-10 Shear Stress Distribution in the Base Layer for 2 Percent Cement Stabilized System (V3) under Wet Conditions....57

Figure 5-11 Shear Strength Ratios for High Fines System V3 under Wet Conditions 60
Figure 5-12 Shear Strength Ratios for 2 Percent Cement Stabilized High Fines System V3 under Wet Conditions 60
Figure 5-13 Finite Element Predictions of Plastic Deformation on the Surface 62
Figure 5-14 Percent Improvement (Loss) of Performance in Terms of Decrease (Increase) of Plastic Deformation at the Pavement Surface 63

LIST OF TABLES

Table 2-1 Particle Size Distribution of Variants....12
Table 2-2 Material Variables and Testing Matrix....14
Table 2-3 ICAR Small Stress Loading Protocol....20
Table 3-1 Moisture Content and Dry Density of Unbound Systems Compacted at Optimum Moisture Content....24
Table 3-2 Moisture Content and Dry Density of Unbound Systems Compacted at Wet....25
Table 3-3 Moisture Content and Dry Density of 1 Percent Cement Stabilized Systems Compacted at Optimum Moisture Content....25
Table 3-4 Moisture Content and Dry Density of 1 Percent Cement Stabilized Systems Compacted at Wet of Optimum Moisture Content....25
Table 3-5 Moisture Content and Dry Density of 2 Percent Cement Stabilized Systems Compacted at Optimum Moisture Content....25
Table 3-6 Moisture Content and Dry Density of 2 Percent Cement Stabilized Systems Compacted at Wet of Optimum Moisture Content....25
Table 3-7 Percent Changes in Anisotropic Resilient Moduli of V3 and V4 with 30
Table 3-8 Percent Changes in Anisotropic Resilient Moduli of Stabilized Systems with Respect to Unbound Systems 30
Table 4-1 Material Parameters of the Aggregate Systems....44
Table 4-2 Finite Element Results of Critical Pavement Responses....45
Table A-1 Anisotropic Material Properties for Gradation V1 at Optimum Moisture Content and with 0 Percent Stabilizer 67
Table A-2 Anisotropic Material Properties for Gradation V2 at Optimum Moisture Content and with 0 Percent Stabilizer 67
Table A-3 Anisotropic Material Properties for Gradation V3 at Optimum Moisture Content and with 0 Percent Stabilizer 67
Table A-4 Anisotropic Material Properties for Gradation V4 at Optimum Moisture Content and with 0 Percent Stabilizer 68
Table A-5 Anisotropic Material Properties for Gradation V1 at Wet of Optimum Moisture State and with 0 Percent Stabilizer....68
Table A-6 Anisotropic Material Properties for Gradation V2 at Wet of Optimum Moisture State and with 0 Percent Stabilizer....68
Table A-7 Anisotropic Material Properties for Gradation V3 at Wet of Optimum Moisture State and with 0 Percent Stabilizer....69
Table A-8 Anisotropic Material Properties for Gradation V1 at Optimum Moisture Content and with 1 Percent Stabilizer 69

Table A-9 Anisotropic Material Properties for Gradation V2 at Optimum Moisture Content and with 1 Percent Stabilizer 69
Table A-10 Anisotropic Material Properties for Gradation V3 at Optimum Moisture Content and with 1 Percent Stabilizer 70
Table A-11 Anisotropic Material Properties for Gradation V4 at Optimum Moisture Content and with 1 Percent Stabilizer 70
Table A-12 Anisotropic Material Properties for Gradation V1 at Wet of Optimum Moisture State and with 1 Percent Stabilizer 70
Table A-13 Anisotropic Material Properties for Gradation V2 at Wet of Optimum Moisture State and with 1 Percent Stabilizer 71
Table A-14 Anisotropic Material Properties for Gradation V3 at Wet of Optimum Moisture State and with 1 Percent Stabilizer 71
Table A-15 Anisotropic Material Properties for Gradation V4 at Wet of Optimum Moisture State and with 1 Percent Stabilizer 71
Table A-16 Anisotropic Material Properties for Gradation V1 at Optimum Moisture Content and with 2 Percent Stabilizer 72
Table A-17 Anisotropic Material Properties for Gradation V2 at Optimum Moisture Content and with 2 Percent Stabilizer 72
Table A-18 Anisotropic Material Properties for Gradation V3 at Optimum Moisture Content and with 2 Percent Stabilizer 72
Table A-19 Anisotropic Material Properties for Gradation V4 at Optimum Moisture Content and with 2 Percent Stabilizer 73
Table A-20 Anisotropic Material Properties for Gradation V1 at Wet of Optimum Moisture State and with 2 Percent Stabilizer 73
Table A-21 Anisotropic Material Properties for Gradation V2 at Wet of Optimum Moisture State and with 2 Percent Stabilizer 73
Table A-22 Anisotropic Material Properties for Gradation V3 at Wet of Optimum Moisture State and with 2 Percent Stabilizer 74
Table A-23 Anisotropic Material Properties for Gradation V4 at Wet of Optimum Moisture State and with 2 Percent Stabilizer 74
Table B-1 Modular Ratios for Gradation V1 at Optimum Moisture Content and with 0 Percent Stabilizer 77
Table B-2 Modular Ratios for Gradation V2 at Optimum Moisture Content and with 0 Percent Stabilizer 77
Table B-3 Modular Ratios for Gradation V3 at Optimum Moisture Content and with 0 Percent Stabilizer 77
Table B-4 Modular Ratios for Gradation V4 at Optimum Moisture Content and with 0 Percent Stabilizer 78

Table B-5 Modular Ratios for Gradation V1 at Wet of Optimum Moisture State and with 0 Percent Stabilizer 78
Table B-6 Modular Ratios for Gradation V2 at Wet of Optimum Moisture State and with 0 Percent Stabilizer 78
Table B-7 Modular Ratios for Gradation V3 at Wet of Optimum Moisture State and with 0 Percent Stabilizer 79
Table B-8 Modular Ratios for Gradation V1 at Optimum Moisture Content and with 1 Percent Stabilizer 79
Table B-9 Modular Ratios for Gradation V2 at Optimum Moisture Content and with 1 Percent Stabilizer 79
Table B-10 Modular Ratios for Gradation V3 at Optimum Moisture Content and with 1 Percent Stabilizer 80
Table B-11 Modular Ratios for Gradation V4 at Optimum Moisture Content and with 1 Percent Stabilizer 80
Table B-12 Modular Ratios for Gradation V1 at Wet of Optimum Moisture State and with 1 Percent Stabilizer 80
Table B-13 Modular Ratios for Gradation V2 at Wet of Optimum Moisture State and with 1 Percent Stabilizer 81
Table B-14 Modular Ratios for Gradation V3 at Wet of Optimum Moisture State and with 1 Percent Stabilizer 81
Table B-15 Modular Ratios for Gradation V4 at Wet of Optimum Moisture State and with 1 Percent Stabilizer 81
Table B-16 Modular Ratios for Gradation V1 at Optimum Moisture Content and with 2 Percent Stabilizer 82
Table B-17 Modular Ratios for Gradation V2 at Optimum Moisture Content and with 2 Percent Stabilizer 82
Table B-18 Modular Ratios for Gradation V3 at Optimum Moisture Content and with 2 Percent Stabilizer 82
Table B-19 Modular Ratios for Gradation V4 at Optimum Moisture Content and with 2 Percent Stabilizer 83
Table B-20 Modular Ratios for Gradation V1 at Wet of Optimum Moisture State and with 2 Percent Stabilizer 83
Table B-21 Modular Ratios for Gradation V2 at Wet of Optimum Moisture State and with 2 Percent Stabilizer 83
Table B-22 Modular Ratios for Gradation V3 at Wet of Optimum Moisture State and with 2 Percent Stabilizer 84
Table B-23 Modular Ratios for Gradation V4 at Wet of Optimum Moisture State and with 2 Percent Stabilizer 84

CHAPTER 1

LITERATURE REVIEW OF FINES

1.1 Background

It is estimated that about 5127 crushed stone quarrying operations and 6000 sand and gravel operations exist in the United States, which produce 2000 million tons of aggregates annually (Bolen, Kalyoncu et al. 1996) he aggregate production industry produces byproduct mineral fine materials in the process of rock crushing. The stockpiling, transportation, and disposal of byproduct fines pose several environmental and financial concerns for the aggregate industry. For civil engineering applications such as the use of fines in bonded and unbounded pavement layers, soil caps, infiltration layers, and general fill, improved knowledge of the characteristics of fines can help to maximize their potential for use in the construction industry.

1.2 Definition of Fines

The definition of fines varies within the industry. The European Aggregates Standards (ESA) defines the fine aggregates as materials passing sieve #4 for use in concrete, as particles smaller than 2 mm for use in asphalt, and as particles smaller than 0.063 mm for use in filler. The general consensus among the aggregate producers in the United States is that fines are the undersized material from crushing plants that is given no further processing and accumulates over time, or material produced by baghouse installations. The maximum size of fines from crushing plants may be as large as 6 mm, and size fractions below this vary greatly. Baghouse fines, which may later be mixed with fines produced during crushing of the parent rock, are typically below 0.075 mm (passing sieve #200). Typically there are two main particle size fractions, materials smaller than 9.5 mm (particles passing sieve 3/8 inch) and particles smaller than 75 microns (passing sieve #200).

1.3 **Types and Amounts Produced**

(Hudson, Little et al. 1997) wrote a comprehensive report on the status of byproduct mineral fines produced by construction aggregates companies in the United States. The report was based on a survey of 154 companies that operate 362 plants around the country. Hudson et al. report that these companies produce about 292 million tons of aggregates annually. From this production level, it was estimated that 478 to 508 million tons of smaller than 9.5 mm mineral fines are produced, 91 to 103 million tons of which are not marketed annually in the United States. Additionally, 103 to 112 million tons of particles smaller than 75 microns (passing sieve #200) mineral fines are produced, and about 76 to 81 million tons are not marketed. Besides the annual production of byproduct mineral fines, it is estimated that 305 to 330 million tons of stockpiled materials smaller than 9.5 mm and about 406 million tons of fines smaller than 75 microns (passing sieve #200) in pond or pit storage are available (Hudson, Little et al. 1997).

According to Hudson the byproduct mineral fines can be categorized into three major groups:

- fines retrieved from dry screening,
- fines retrieved from wet screening or from settling ponds, and
- baghouse fines.

The collection of mineral fines varies depending on the facilities that collect the fines in the quarry. The two major types are dry processing and wet processing. Aggregate particles retrieved from dry screenings are usually smaller than 5 mm in size and accumulate during primary and secondary crushing and separation. About 5 to 10 percent of byproduct fines originate from dry-screening operations. The chemical and mineralogical contents of screenings depend on the mineral types in the gravel or parent rock. The physical characteristics of the byproduct fines such as fine particle angularity may vary because of variations in mineralogy, strength, and fracture characteristics of the aggregates or the parent rock as well as the crushing techniques used in the quarries.

Quarries that operate as dry plants retrieve the fines in the screening operations and also from baghouses or cyclones. According to the study by Hudson et al. (1997) on the state of fines production in the United States, baghouse fines represent about 5 percent of the mineral fines generated and are typically smaller than 75 microns. Baghouse fines are collected dry; therefore, they present less of a handling concern than damp or wet byproduct fines.

Sediment fines in ponds or settling pond fines, pond screenings, pond slime, and pond tailings are obtained from washing aggregate as it is wet-processed into a product. These fines represent about 10 to 15 percent of the total aggregate production. Pond fines are usually directed to a settling tank or hydraulic cyclone where the coarser fractions can be removed for further industry use and the remaining fines are discharged into a series of sequential settling ponds.

Currently, the aggregates and crushed rock industries are moving toward using more wet-processing operations due to environmental and air pollution concerns rather than dry crushing. Therefore, depending on the type of facility and the scope of operation, the byproduct fines can be collected through wet or dry screenings.

The handling, stockpiling, and disposal of aggregate byproduct mineral fines are costly. It has been estimated that the handling and disposal of pond screenings cost the industry about $400 million annually (Machemehl 1996). This cost includes removing, drying, and transporting the pond fines to stockpiles or for further industry use.

A number of industry-sponsored studies have examined the current and potential utilization of mineral fines. According to (Hudson, Little et al. 1997), current uses of mineral fines include:

- pavement and geotechnical engineering uses such as high fines aggregate bases, asphalt pavement layers with elevated fines content, high fines concrete, and backfills;

- agricultural uses such as Aglime and fertilizer filler;
- environmental uses of limestone aggregate fines to control SO_2 emissions, pond and watershed liming, acid mine drainage abatement, and landfill layers; and
- miscellaneous applications such as industrial fillers and paints.

According to a study conducted by (Wood 1995) possible uses of mineral fines include asphalt concrete products, Portland cement products, chemical products, industrial minerals, mineral coatings, fillers and pigments, environmental and pollution control products (such as acid neutralization, landfill daily cover, and sludge dewatering aid), and ceramic products.

1.4 **Civil Engineering Applications of Waste or Byproduct Fines, Review of Literature**

Aggregate bases are a significant potential use of quarry fines. According to Rockliff , the wider use of byproduct quarry fines in unbound aggregate layers in highway pavements may have been held back by insufficient specifications (D. Rockliff 1996).

The study conducted by (Touahamia, Sivakumar et al. 2002) indicates that quarry fines can be substituted for primary aggregate used as coarse granular material for backfilling, highway construction, and sub-bases for roads and railway tracks. The authors constructed compacted layers of the dry quarry waste, building debris, and crushed concrete separated by geogrids. The strength and performance of the layers made of waste materials and byproduct fines were evaluated and compared to traditional aggregate layers made of crushed basalt. The authors reported that the quarry waste had a much smaller particle size distribution than the other materials (smaller than 5 mm as opposed to smaller than 13 mm waste materials). This study found that the presence of geosynthetic reinforcement layers greatly increased the shear strength (by up to 50 percent) and resulted in smaller plastic deformations.

Parker reported a similar study investigating the advantages of utilizing fines generated in the crushing process as engineered backfill for mechanically stabilized earth walls. Three materials—granite screenings, limestone pond fines, and natural pit run sand—were

tested for strength, permeability, and chemical properties. A 12-foot-high geotextile fabric–stabilized wall was designed using the measured properties, and the author reported that crushed stone fines required less fabric reinforcement than natural sand, resulting in less construction costs (Parker 1996).

In another study by De Rezende and De Carvalho in 2003 on the utilization of quarry waste in highway pavements, a test section 240 feet long and 30 feet wide was constructed in a low-traffic zone, and the performance was monitored over a three-year period. Quarry waste with a grain size of smaller than 100 mm was used to construct an 8-inch-thick base layer, which was covered by a 2.5-inch asphalt layer. The performance results from this test section showed that the quarry waste can be used successfully as a base for low-volume highway facilities (De Rezende and De Carvalho 2003).

Where soil erosion and land gradients are a problem for land developers, fines can be an attractive alternative to soil backfill. Waste fines are more easily worked than highly plastic clay soils, benefiting the contractors. A test project was carried out in Georgia in 1988 by Vulcan Materials Company, using backfill for the building of a large mall (Brown 1996). Brown reported that the fines from Vulcan Materials' Kennesaw quarry could withstand the required bearing pressures of 4000 psf. He also reported that the moisture density, safety factor for bearing capacity, void ratio, and angularity of the waste fines were also suitable. The material allowed quick and economical construction of a large fill project in an urban area.

Several researchers have studied the resilient behavior of high fines unbound systems. These studies reported a decrease in the resilient modulus due to an increase in fines content (Thadkamalla and George. 1995; Simonsen, Janoo et al. 2002) and (Gray 1962). Gray reported that in unbound aggregate bases with 25.4 mm maximum particle size, the highest strength was achieved through the use of a maximum of 8 percent fines. (Tutumluer and Seyhan 1999) evaluated the anisotropic resilient properties of aggregate systems and reported that the aggregate matrix showed significant softening behavior as the percentage of fine particles (materials smaller than 75 microns) exceeded 12 percent.

High fines base layers were shown to be sensitive to moisture variation and susceptible to frost heave. Simonson studied the effect of freeze-thaw cycles on fine-grained soils. They performed resilient modulus tests on samples frozen at $-10^{o}C$ in triaxial cells, then thawed the samples before testing, and found a 50 percent reduction in vertical resilient modulus values (Simonsen, Janoo et al. 2002).

Thadkamalla studied the effect of moisture and saturation techniques on the resilient behavior of coarse and fine-grained soils. Their study concluded that the saturation level above the optimum moisture content has a nominal effect (20 percent reduction) on the vertical resilient modulus in coarse-grained soils, whereas it has a severe effect (50 to 75 percent reduction) on fine-grained subgrades (Thadkamalla and George. 1995).

1.5 **Impact of Lithology on Fines Generation**

The recent study conducted by (Manning and Vetterlein 2004) on exploitation of quarry fines in Great Britain indicates that construction aggregates produced by crushing of limestone rock (including dolomite and chalk) typically produce around 20 to 25 percent fines in the crushing process, whereas sandstone quarries produce up to 35 percent fines. Manning et al. reported that the strength and physical properties of fine particles generated from sand and gravel pits vary enormously depending on the sand-to-gravel ratio and on the clay content, but are mostly between 5 to 15 percent of production. Igneous rocks are also variable based on the lithology of the aggregates, and the byproduct fines generated in the crushing process range from 10 to 30 percent. Manning reported that according to a British geological survey report published in 2003, the total annual production of construction aggregates is around 238 million tons; therefore, the total annual production of quarry fines in Great Britain is estimated to be on the order of 41 million tons (Manning and Vetterlein 2004).

Figure 1-1 and Figure 1-2 show the impact of lithology of the aggregates on the generation of byproduct fines during plant operations in Great Britain. Figure 1-1 summarizes the annual production of construction aggregates based on tonnage of final products. Figure 1-2 demonstrates the impact of mineralogy and the source of the parent rock on the generation of quarry fines.

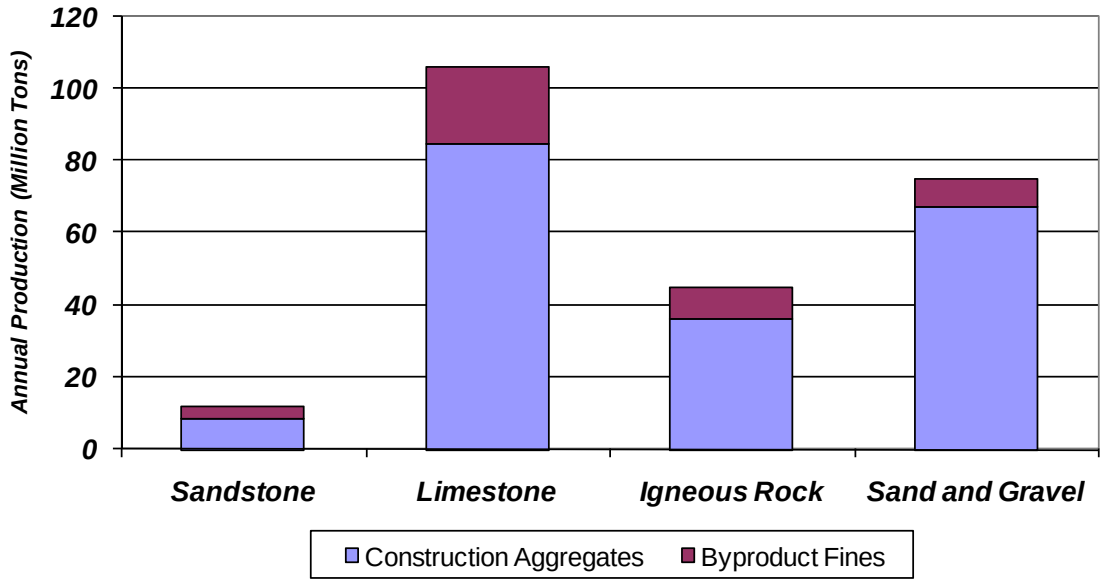

Figure 1-1 Impact of Lithology on Fines Generation Based on Weight

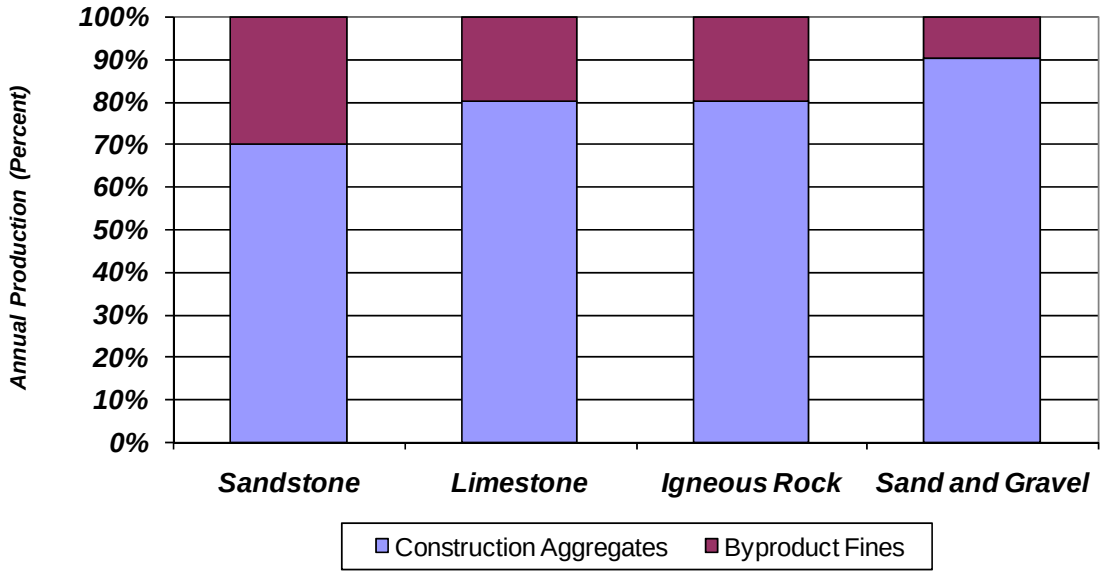

Figure 1-2 Impact of Lithology on Fines Generation Based on Percentage

The generation of byproduct fines in the operation process is also a function of crushing techniques used in the plant. The next section of this report presents the different types of crushing and their impact on fines generation.

1.6 **Impact of Crusher Type in Fines Generation**

The quarry operation's final product—construction aggregates—is produced by abrasion/attrition of the parent rock as it comes into contact with other rock particles; this is a result of fracture of the rock in weak planes as the particles smash past each other. As a result of this impact, crushers tend to produce less flat and elongated particles and more particles more angular aggregates. The major drawback of these crushers is the fact that, due to the impact, more fines are produced during plant operation. Hudson et al. (1997) reported that impact crushers on average generate 20 to 25 percent more fine particles compared to compressive crushers.

In an another study at Georgian Aggregate's Duntroon Quarry in Toronto, Canada, Seberras reported that when the primary crusher had changed from an impact crusher to a jaw crusher, the plant produced 28 percent fines in lieu of 38 percent fines, equivalent to a reduction of 100,000 metric tons per year (tpa) (Seberras 2000).

Bateman reported that when Dufferin Aggregate replaced its vertical shaft impact crusher with a cone crusher, they reduced the byproduct fines production and enhanced the performance of the quarry. He reported that upon this change, they increased their production of single-size aggregates from 40 to 50 percent by weight of the total plant production (Bateman 2003).

1.7 **Issues with the Crushers**

In a report by Manning on the exploitation of quarry fines in Great Britain, the authors summarized the issues with crushers and plant operations that cause an increase in fines generation as follows (Manning and Vetterlein 2004):

- The proportion of filler-grade material produced by an impact crusher ranges from 5 to 20 percent. This proportion increases as the operation speed in the plant increases (Ahn and Fowler 1999).
- Feeding the crusher too fast will cause a significant increase in fines generation due to the elevated probability of rock-on-rock interaction in the crushing chamber.
- Scalping of the primary crushed material increases the capacity of the subsequent crushing stages and reduces the likelihood of material becoming wedged in the crushers (known as “packing”). Packing can lead to excess fines being produced due to the greater rock-on-rock interaction.

CHAPTER 2

LABORATORY TESTS AND MATERIALS

2.1 Materials and Experimental Variables

Four gradations of limestone aggregates sourced from Brownwood, Texas, were selected to study the synergistic impact of fines, moisture, and light stabilization of aggregate systems. Aggregate gradations were selected to have different percentages of fines passing sieve #40 (425 microns). It is important to note that the gradations were selected in order to provide enough intermediate aggregate particles in fine gradations to maintain proper packing and aggregate interlock. Gradation V1, which follows the ASTM D2940-03, Standard Specification for Graded Aggregate Material for Bases or Subbases for Highways or Airports, designation, was selected as the reference gradation in this study. The impact of fines and stabilizers as well as moisture state on the mechanical properties of the aggregate systems were later determined and compared to the V1 gradation. The fine aggregate fraction was increased incrementally to form gradations V2 (20 percent fines), V3 (30 percent fines), and V4 (40 percent fines). The percentages of intermediate particle sizes were adjusted to maintain appropriate density in each gradation variant. The gradations of the systems evaluated in this study and ASTM D2940 requirements for base gradation are shown in Table 2-1. Particle size distributions are presented in Figure 2-1.

2.2 Material Tests

The following tests were performed on the samples to investigate the synergistic effect of fines, moisture, and stabilizer on the performance of high fine aggregate systems:

- Atterberg limits,
- moisture density test,

- anisotropic triaxial test,
- repeated load permanent deformation test,
- unconfined compressive strength test, and
- aggregate shape properties using AIMS and electronic light microscope.

Table 2-1 Particle Size Distribution of Variants

Sieve Opening (mm)	sieve No.	*Percent Passing (%)*				
		ASTM D-2940	***V1***	***V2***	***V3***	***V4***
37.5	1.5	95-100	100	100	100	100
19	3/4	70-92	85	85	85	90
9.5	3/8	50-70	60	65	75	80
4.75	4	35-55	40	50	60	65
2.36	8	…	25	35	50	55
1.18	16	…	20	30	40	50
0.600	30	12-25	…	…	…	…
0.425	40	…	15	20	30	40
0.15	100	…	10	15	20	30
0.075	200	0-8	5	10	15	20

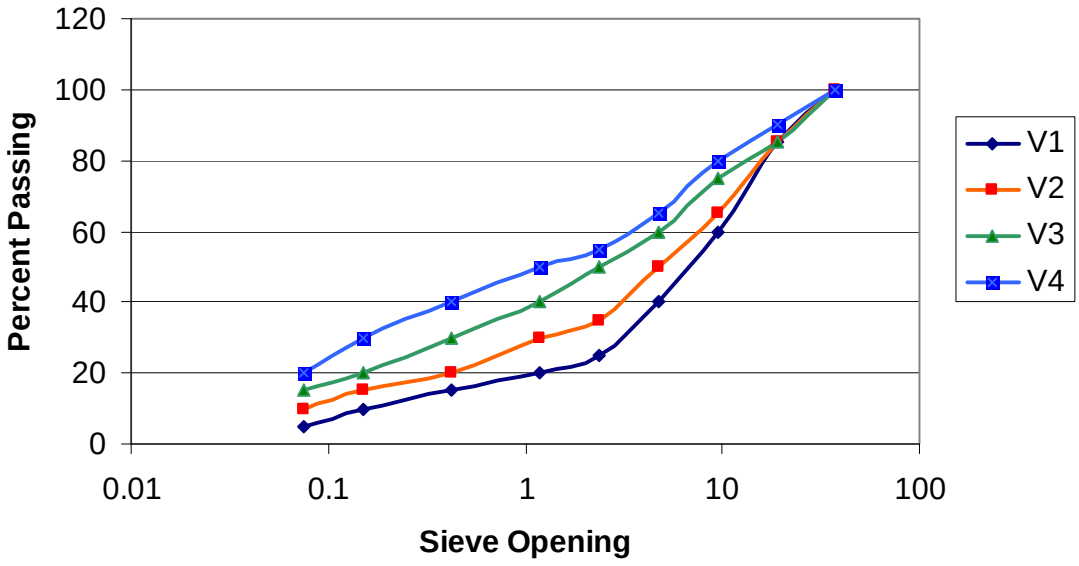

Figure 2-1 Particle Size Distributions

In order to evaluate the impact of low levels of stabilization, either 1 or 2 percent of type I cement was added to the selected aggregate systems in the factorial. Samples were prepared using the impact compaction method following AASHTO T-180 using a 4.54 kg hammer and a 457 mm drop. Samples were compacted in rigid cylindrical molds 150 mm in diameter and 150 mm in height, in three 50 mm thick layers, by applying 25 blows per layer.

2.3 Specimen Conditioning

Resilient properties and permanent deformation properties were measured on specimens compacted at optimum and wet of optimum (optimum + 2 percent) volumetric water contents. The compressive strength was measured on specimens compacted at optimum moisture content but subjected to moisture conditioning as described later in this report. The variation in water content was used in order to study the moisture susceptibility of aggregate systems containing excess amounts of low-plasticity fine particles. The Plasticity Index (PI) of the Texas limestone used in this study was 8 percent. In order to study the effect of moisture on the mechanical response of the aggregates, the materials were tested in three moisture conditions: optimum moisture content, dry of optimum moisture content, and wet of optimum moisture content. A compaction test (ASTM D1557) was performed on the aggregates to determine the optimum water content of each gradation variant.

As shown in Table 2-2, testing was conducted on different permutations of material conditions in order to evaluate the synergistic effect of fines content, moisture state, and stabilizer content on the engineering properties of high fine aggregate systems.

Table 2-2 Material Variables and Testing Matrix

Test	*Material Condition*		
	Gradation (Percent Fines Passing Sieve #40)	***Percent of Stabilizer***	***Moisture State***
Resilient Properties	V1 (15%) V2 (20%) V3 (30%) V4 (40%)	0% 1% 2%	Optimum, Wet of Optimum (Optimum + 2%)
Permanent Deformation	V1 (15%) V2 (20%) V3 (30%) V4 (40%)	0% 1% 2%	Optimum, Wet of Optimum (Optimum + 2%)
Compressive Strength	V1 (15%) V2 (20%) V3 (30%) V4 (40%)	0% 1% 2%	Optimum & Moisture Conditioning

The main mode of stabilization of the fines with low levels of Portland cement (1 and 2 percent) is to develop a cement matrix primarily of calcium silicate hydrate (CSH) among the fine aggregate. However, since the concentration of calcium due to the addition of Portland cement is high in the fines matrix of limestone particles, it is probable that a calcium carbonate matrix may also be developed *(9)*. Major strength improvements can be achieved through time dependant soil-cement and pozzolanic reactions. This objective was investigated with the strength gain process in samples tested for unconfined compressive strength.

With the intention of simulating the early and critical stages of performance, aggregate systems were tested for anisotropic resilient properties and permanent deformation potential immediately after compaction. Substantial further improvements in resilient response and rutting potential of stabilized systems are expected through time dependent strength gain reactions by forming CSH and calcium aluminate hydrate (CAH) products.

2.4 **Laboratory Tests for Mechanical Behavior of Aggregates**

In order to assess the complex behavior and directional dependency of the response of aggregate bases under a moving wheel load, aggregate samples were tested following the International Center for Aggregates Research (ICAR) small strain protocol. Figure 2-2 schematically illustrates the stress paths applied to aggregate samples using the ICAR approach.

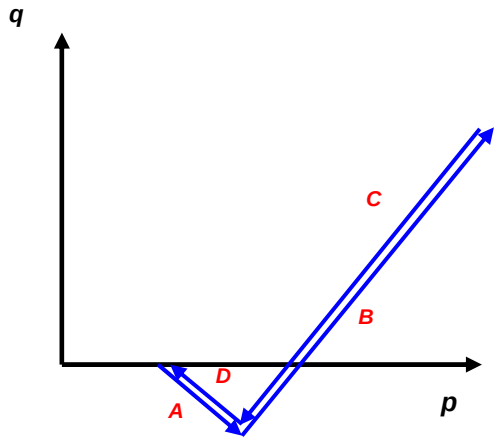

Figure 2-2 Stress Path Induced by Moving Wheel on Pavement

The repeated load triaxial tests have been widely used to simulate the stress states applied by traffic load on aggregate layers. The standard triaxial test protocols were only suitable for simulating the state of the stresses under stationary load. A proper test protocol should be used to capture the extension-compression-extension stress regimens induced by moving wheel load on the aggregate layer. This loading regimen is presented in Figure 2-2. As the wheel approaches the reference point, more confinement is induced on the pavement, and as it departs the reference point, the magnitude of confinement decreases. The same behavior is valid for the vertical stresses. The pavement experiences the highest vertical stress when the wheel load is directly on the reference point, and as it departs, the value diminishes. This constant change in the vertical and horizontal stresses causes rotation of the direction of principal stresses. Therefore, using triaxial loading protocols that use a constant confining pressure (CCP) stress path does not realistically simulate the stresses induced by moving traffic load. Variable dynamic confining

pressure (VDCP)–type repeated load triaxial tests offer the possibility of applying dynamic vertical and horizontal stresses individually and controlling the magnitude of the confining pressure along each stress path. Researchers used the ICAR small strain VDCP loading protocol to investigate the anisotropic behavior of stabilized high fines systems.

In this study, the RaTT (rapid triaxial test) cell developed by Industrial Process Controls (IPC) in Australia was used for testing the specimens (Figure 2-3). The main advantage of this test equipment is that the rubber membrane inside the RaTT cell can be automatically controlled by a computer to apply both static and dynamic confining pressure to the samples. The RaTT cell can apply both static and dynamic loadings individually in horizontal and vertical directions.

The IPC system supports automated cell movement and displacement measurement with linear variable differential transducers (LVDT) for both directions.

Figure 2-3 RaTT Cell Assembly

2.5 **Testing Protocol**

There are five anisotropic elastic properties needed to characterize the anisotropic behavior of the aggregates. In order to solve for these five properties, a test protocol was developed by researchers in the ICAR/502 project. This test protocol assumes that the elastic modulus follows the Uzan model and the nonlinear tangential moduli are a smooth function of stress invariants. It was also assumed that the variations of these tangential moduli are negligible within small changes in the state of the stresses so the behavior of the material stays elastic. The ICAR test protocol uses three stress regimes: compression, shear, and extension.

This protocol provides a means to determine cross-anisotropic material properties: E_x and E_y (elastic modulus in the horizontal and vertical directions, respectively), ν_{xy} and ν_{xx} (Poisson's ratio in the horizontal direction due to vertical loading and Poisson's ratio in the horizontal direction due to horizontal loading, respectively), and G_{xy} (shear modulus). Applied stresses and measured strains were then input into an iterative error minimization toolkit using a system identification method to simultaneously solve for four of the five anisotropic material properties (E_x, E_y, ν_{xx}, and ν_{xy}).

$$\begin{bmatrix} \frac{1}{E_x} & -\frac{\nu_{xy}}{E_x} & -\frac{\nu_{xx}}{E_x} \\ -\frac{\nu_{xy}}{E_x} & \frac{1}{E_y} & -\frac{\nu_{xy}}{E_x} \end{bmatrix} \begin{bmatrix} \sigma_x \\ \sigma_y \\ \sigma_x \end{bmatrix} = \begin{bmatrix} \varepsilon_x \\ \varepsilon_y \end{bmatrix} \tag{2-1}$$

The fifth material property, G_{xy}, was directly determined using elastic work potential relationships derived specifically for the shear stress regimen and presented in equation 2-2. Details regarding the derivation of equation 2-2 can be found in Kumar and Hudson *(2)*.

$$G_{xy} = \frac{3}{4} \frac{\Delta\sigma_y}{(\Delta\varepsilon_y - \Delta\varepsilon_x)} \tag{2-2}$$

2.6 **Compression Regime**

In this test mode, the confining stress at each stress state is kept constant while the axial stress is increased by $\Delta\sigma y^c$. Thus, the sample is loaded to (σ_y^c, σ_x^c), reloaded to (σy^c + $\Delta\sigma y^c$, $\Delta\sigma x^c$), and unloaded back to (σy^c, $\Delta\sigma x^c$) for each cycle.

$$\begin{bmatrix} \frac{1}{E_x} & -\frac{\nu_{xy}}{E_x} & -\frac{\nu_{xx}}{E_x} \\ -\frac{\nu_{xy}}{E_x} & \frac{1}{E_y} & -\frac{\nu_{xy}}{E_x} \end{bmatrix} \begin{Bmatrix} \Delta\sigma_x^c \\ \Delta\sigma_y^c \\ \Delta\sigma_x^c \end{Bmatrix} = \begin{Bmatrix} \Delta\varepsilon_x^c \\ \\ \Delta\varepsilon_y^c \end{Bmatrix} \tag{2-3}$$

where:

- $\Delta\varepsilon x^c$ = a change in radial strain due to an infinitesimal change in axial stress $\Delta\sigma y^c$ in triaxial compression,
- $\Delta\varepsilon y^c$ = a change in axial strain due to an infinitesimal change in axial stress $\Delta\sigma y^c$ in triaxial compression, and
- $\Delta\sigma x^c = 0$.

2.7 **Shear Regime**

In this phase of the test, the axial stress is increased slightly by $\Delta\sigma_y^s$, and the confining stress is decreased by $\Delta\sigma_x^s = ½\ \Delta\sigma_y^s$. Thus, at the stress state (σ_y^s, σ_x^s), the sample is loaded to ($\sigma_y^s + \Delta\sigma_y^s$, $\sigma_x^s - \Delta\sigma_x^s$) and unloaded back to ($\sigma_y^s$, σ_x^s) in each cycle. This way, there is no change in the first stress invariant, I.

$$\begin{bmatrix} \frac{1}{E_x} & -\frac{\nu_{xy}}{E_x} & -\frac{\nu_{xx}}{E_x} \\ -\frac{\nu_{xy}}{E_x} & \frac{1}{E_y} & -\frac{\nu_{xy}}{E_x} \end{bmatrix} \begin{Bmatrix} \Delta\sigma_x^s \\ \Delta\sigma_y^s \\ \Delta\sigma_x^s \end{Bmatrix} = \begin{Bmatrix} \Delta\varepsilon_x^s \\ \\ \Delta\varepsilon_y^s \end{Bmatrix} \tag{2-4}$$

2.8 **Extension Regime**

In this phase of the test, there is a slight decrease in the axial stress by $\Delta\sigma y^{\varepsilon}$ and a slight increase in the confining stress by $\Delta\sigma x^{\varepsilon}$. Thus, at the stress state (σy^{ε}, σx^{ε}), the sample is loaded to ($\sigma y^{\varepsilon} - \Delta\sigma y^{\varepsilon}$, $\sigma x^{\varepsilon} + \Delta\sigma x^{\varepsilon}$) and unloaded back to ($\sigma y^{\varepsilon}$, σx^{ε}) in each cycle.

$$\begin{bmatrix} \frac{1}{E_x} & -\frac{\nu_{xy}}{E_x} & -\frac{\nu_{xx}}{E_x} \\ -\frac{\nu_{xy}}{E_x} & \frac{1}{E_y} & -\frac{\nu_{xy}}{E_x} \end{bmatrix} \begin{Bmatrix} \Delta\sigma_x^e \\ \Delta\sigma_y^e \\ \Delta\sigma_x^e \end{Bmatrix} = \begin{Bmatrix} \Delta\varepsilon_x^e \\ \\ \Delta\varepsilon_y^e \end{Bmatrix} \tag{2-5}$$

where:

- $\Delta\varepsilon x^{\varepsilon}$ = a change in radial strain due to an infinitesimal change in axial stress $\Delta\sigma y^{c}$ and radial stress $\Delta\sigma x^{\varepsilon}$, and
- $\Delta\varepsilon y^{c}$ = a change in axial strain due to an infinitesimal change in axial stress $\Delta\sigma y^{c}$ and radial stress $\Delta\sigma x^{\varepsilon}$.

The stresses applied and the strains obtained from the three stress regimes described above are used in a system identification scheme to determine the five cross-anisotropic parameters.

At each static stress state, small dynamic changes in stresses are applied to obtain three triaxial stress regimes such that the net stress changes represent triaxial compression, triaxial shear, and triaxial extension. A loading cycle of dynamic stress consists of 1.5 seconds of loading and 1.5 seconds of unloading. As for sample conditioning, a dynamic loading is applied to a sample for 25 repetitions until a stable resilient strain is achieved. The resilient axial and radial strains are determined for each stress regime and implemented in the system identification scheme to back-calculate the five anisotropic

elastic properties at that particular stress state. The small stress loading protocol is presented in Table 2-3, and the stress path plot is presented in Figure 2-4.

Table 2-3 ICAR Small Stress Loading Protocol

	Static Stress (Kpa)		Dynamic stress (Kpa)					
			Compression		Shear		Extension	
Stress state	σ_y	σ_x	$\Delta\sigma_y^c$	$\Delta\sigma_x^c$	$\Delta\sigma_y^s$	$\Delta\sigma_x^s$	$\Delta\sigma_y^e$	$\Delta\sigma_x^e$
1	40	25	5	0	10	-5	-5	5
2	50	25	10	0	10	-5	-10	10
3	70	40	10	0	10	-5	-10	10
4	130	60	20	0	20	-10	-10	10
5	150	70	20	0	20	-10	-10	10
6	170	100	20	0	20	-10	-20	20
7	220	120	30	0	30	-15	-20	20
8	250	140	30	0	30	-15	-20	20
9	250	120	30	0	30	-15	-20	20
10	250	105	30	0	30	-15	-20	20

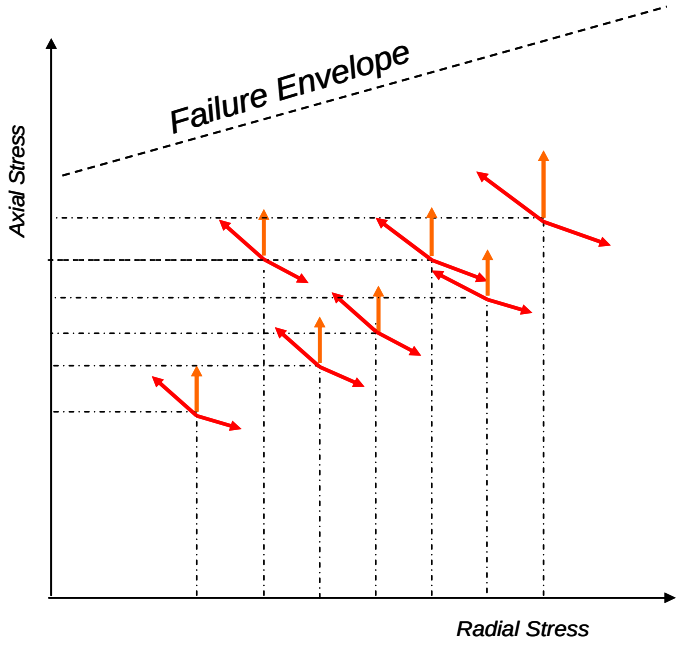

Figure 2-4 Stress Path for ICAR Test Protocol

2.9 **Permanent Deformation Potential**

The permanent deformation test was performed on the aggregate samples approximately 2 hours after compaction without allowing the full strength gain process to take place through the process of pozzolanic reactions and formation of CSH and CAH. The samples were tested at a 50 kPa confining pressure and under a 250 kPa dynamic axial stress using a haversine-shaped 0.1-second load pulse and 0.9-second rest period. The repeated load testing was conducted using a confining pressure of 50 kPa, which is less than the pressure (103.5 kPa) recommended by the NCHRP 1-27 protocol. The lower confining pressure was used to test the systems at critical conditions where more softening of the aggregate matrix occurs, which results in more permanent strain development in the samples. Also, field measurements of lateral pressure induced by wheel loads on instrumented pavement sections resulted in lateral pressures in the range of 35 kPa to 56 kPa in the base layer *(15).* Permanent deformation tests continued for 10,000 cycles, until the specimens failed, or until permanent strain reached 10 percent, whichever occurred first. The unbound high fine aggregate systems (V3 and V4) under wet conditions reached the maximum strain criterion, so these tests were terminated before completion of the10,000 load repetitions.

2.10 **Unconfined Compressive Strength Properties**

As opposed to the resilient modulus and permanent deformation tests, the unconfined compressive strength test was performed on specimens that were compacted at optimum moisture content. However, these specimens were subjected to capillary soak and conditioned in the moisture room at 32^{o}C and 95 percent relative humidity for 48 hours to ensure moisture equilibrium throughout the entire sample. Capillary soak and moisture conditioning of the samples probably triggered some hydration of cement and added to strength gain.

The test was performed in accordance with ASTM D1633-00**.** Specimens were tested in the strain-controlled mode with the strain rate equal to 1 percent per minute. The test was

terminated if a sample experienced 5 percent strain or softening occurred to a point where the stress level decreased to about 80 percent of the peak strength.

CHAPTER 3

LABORATORY TEST RESULTS AND ANALYSIS

3.1 Materials Tested

Four gradation variants of Texas limestone with fines content (particles smaller than 75 microns) ranging from 5 to 20 percent sourced from Brownwood were used in this study. Aggregate systems were tested in three moisture states, namely dry of optimum, optimum, and wet of optimum. Small percentages of type I cement were incrementally added to the aggregate systems. The aggregate systems were tested as unbound (no stabilizer), with 1 percent and 2 percent type I cement, and with different fines contents and moisture contents to study the synergistic effect of moisture, fines, and stabilizer on the anisotropic response of aggregate systems (Figure 3-1).

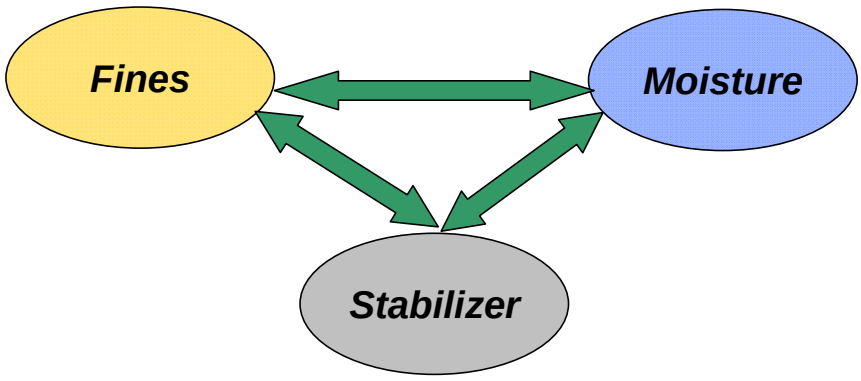

Figure 3-1 Schematic Representation of Synergistic Interaction of Stabilizer, Moisture Content, and Fines Content

3.2 Volumetric Relations

The AASHTO T-180 test procedure was used to prepare the samples in this study. This method uses a 4.45 kg hammer and a 457 mm drop to simulate field compaction in the lab. Samples were compacted in aluminum cylindrical molds 150 mm in diameter and 150 mm in height, in three 50 mm thick layers, by applying 25 blows per layer.

After the samples are extruded from the aluminum molds, the samples' weight, diameter, and height were measured and used for calculating the density of the samples after compaction.

Upon terminating the tests, samples were weighed again and placed in the oven for 48 hours. The dry weights were later used to calculate the dry density and void ratio of the specimens, which are presented in Table 3-1 through Table 3-6. The following relations were used to calculate the dry density and void ratio of the samples:

$$\gamma_{dry} = \frac{\gamma_{total}}{1+\omega} \tag{3-1}$$

$$S_r = \frac{V_v}{V_s} \tag{3-2}$$

$$e = \frac{G_s \omega}{S_r} \tag{3-3}$$

where:

γ_{dry} = dry density (kg/m^3),

ω = water content (%),

γ_{total} = total density (total weight/total volume) (kg/m^3),

V_v = volume of voids in the sample (total volume – volume of soil) (m^3),

V_s = volume of soil in the sample (m^3),

e = void ratio, and

G_s = specific gravity.

Table 3-1 Moisture Content and Dry Density of Unbound Systems Compacted at Optimum Moisture Content

Unbound @ Wet of Optimum

	Gradation V1	*Gradation V2*	*Gradation V3*	*Gradation V4*
Achived Moisture Content(%)	7.8	8.3	8.8	9.1
Dry Density(kg/m^3)	1891	1886	1948	1851
Void Ratio(%)	0.40	0.40	0.36	0.43

Table 3-2 Moisture Content and Dry Density of Unbound Systems Compacted at Wet of Optimum Moisture

Unbound @ Wet of Optimum

	Gradation V1	*Gradation V2*	*Gradation V3*	*Gradation V4*
Achived Moisture Content(%)	7.8	8.3	8.8	9.1
Dry Density(kg/m^3)	1891	1886	1948	1851
Void Ratio(%)	0.40	0.40	0.36	0.43

Table 3-3 Moisture Content and Dry Density of 1 Percent Cement Stabilized Systems Compacted at Optimum Moisture Content

1% Cement Stabilized @ Optimum Target Moisture

	Gradation V1	*Gradation V2*	*Gradation V3*	*Gradation V4*
Achived Moisture Content(%)	6.5	7.4	8.1	9.0
Dry Density(kg/m^3)	2198	2159	2119	2123
Void Ratio(%)	0.21	0.23	0.25	0.25

Table 3-4 Moisture Content and Dry Density of 1 Percent Cement Stabilized Systems Compacted at Wet of Optimum Moisture Content

1% Cement Stabilized @ Wet of Optimum

	Gradation V1	*Gradation V2*	*Gradation V3*	*Gradation V4*
Achived Moisture Content(%)	10.0	11.4	13.6	10.4
Dry Density(kg/m^3)	1934	2082	2181	2065
Void Ratio(%)	0.37	0.27	0.22	0.28

Table 3-5 Moisture Content and Dry Density of 2 Percent Cement Stabilized Systems Compacted at Optimum Moisture Content

2% Cement Stabilized @ Optimum Target Moisture

	Gradation V1	*Gradation V2*	*Gradation V3*	*Gradation V4*
Achived Moisture Content(%)	5.8	8.1	7.7	8.8
Dry Density(kg/m^3)	2065	1875	2003	2000
Void Ratio(%)	0.28	0.32	0.32	0.33

Table 3-6 Moisture Content and Dry Density of 2 Percent Cement Stabilized Systems Compacted at Wet of Optimum Moisture Content

2% Cement Stabilized @ Wet of Optimum

	Gradation V1	*Gradation V2*	*Gradation V3*	*Gradation V4*
Achived Moisture Content(%)	9.9	11.0	13.5	15.0
Dry Density(kg/m^3)	2158	2117	1997	1855
Void Ratio(%)	0.23	0.25	0.33	0.43

Figure 3-2 through Figure 3-4 shows the impact of stabilization and moisture content on the dry densities of the samples.

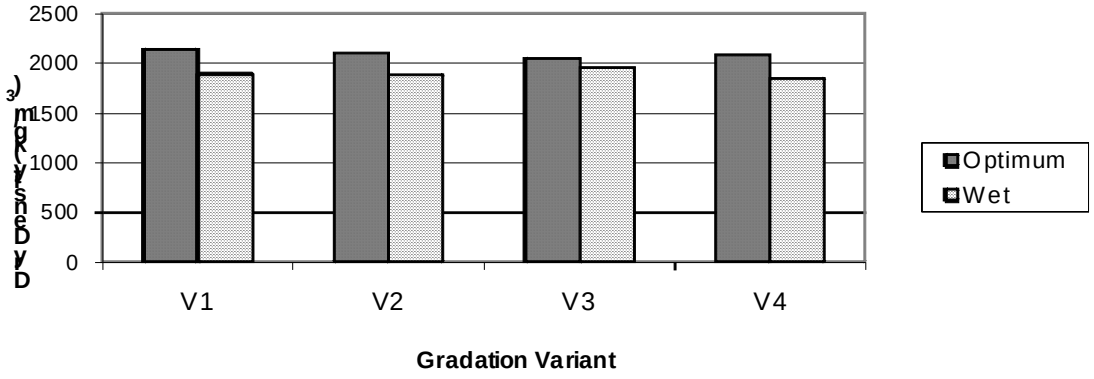

Figure 3-2 Dry Densities of Unstabilized Systems Compacted in Optimum and Wet of Optimum Moisture Conditions

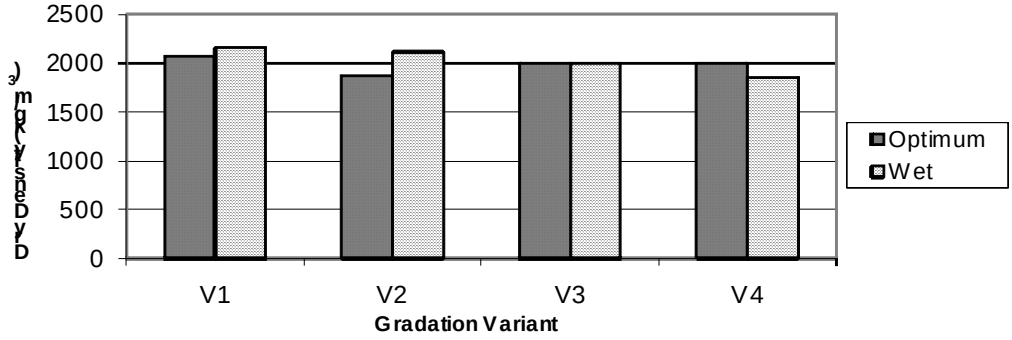

Figure 3-3 Dry Densities of 1 Percent Cement Stabilized Systems Compacted in Optimum and Wet of Optimum Moisture Conditions

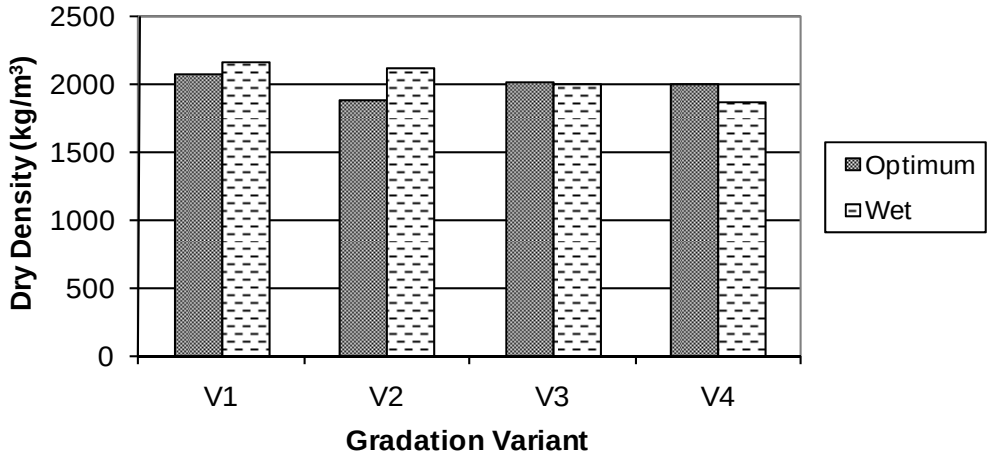

Figure 3-4 Dry Densities of 2 Percent Cement Stabilized Systems Compacted in Optimum and Wet of Optimum Moisture Conditions

As illustrated in Figure 3-2, in unbound systems, samples compacted at 2 percent above the optimum moisture content have lower dry densities compared to the samples compacted at optimum moisture content. Dry densities of control gradations V1 and V2 (within the range of ASTM D2940) at optimum moisture content were found to be higher than V3 and V4 (high fines gradations). Figure 3-2 also shows that gradation V4 (with 20 percent passing sieve #200) at wet conditions has the lowest dry density compared to other samples in unbound conditions. This figure clearly shows the reduction in the dry density of samples due to the coupled effect of high fines content and high saturation levels in unbound aggregate systems.

Figure 3-3 and Figure 3-4 show the impact of stabilizers on the dry density of aggregate systems at optimum and wet of optimum conditions. Figure 3-3 shows that, in all variants except for gradation V3 with 1 percent cement, the achieved dry density in the optimum moisture state was higher than in the wet condition. A plausible explanation for this is that the very low percentage of cement acted more as a filler itself. In gradation V4 where too much fines are present, the 1 percent cement was not enough to act as a bonding

agent and provide better packing between particles. Figure 3-4 shows the dry densities of aggregate systems when 2 percent was present in the mix. The general trend for gradation V1, V2, and V3 shows that stabilized wet systems have higher dry densities compared to their optimum counterparts. This could be explained by the fact that there is enough stabilizer in the mix to form a stabilized matrix that contributes to better packing of the samples. As for gradation V4 with 20 percent passing sieve #200 and 40 percent passing sieve #40, it is observed that the impact of fines is dominant in determining the final density of this variant

Figure 3-5 and Figure 3-6 present another representation of the dry densities categorized and plotted based on moisture state. One important observation derived from Figure 3-6 is that when enough water is present in the mix, the early stages of pozzolanic reactions take place and cause tighter packing of the aggregate particles.

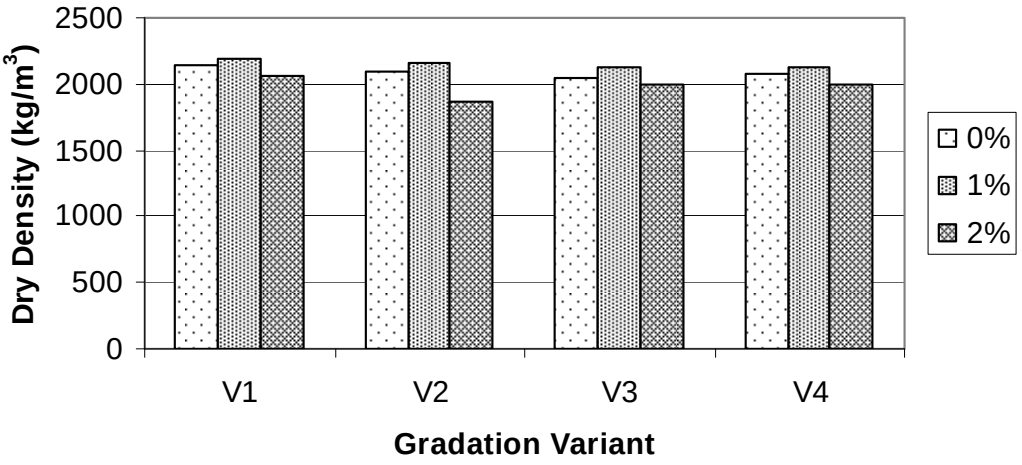

Figure 3-5 Impact of the Variation of Fines Content and Stabilizer Content on the Dry Density of Aggregate Systems Molded at Optimum Moisture Content

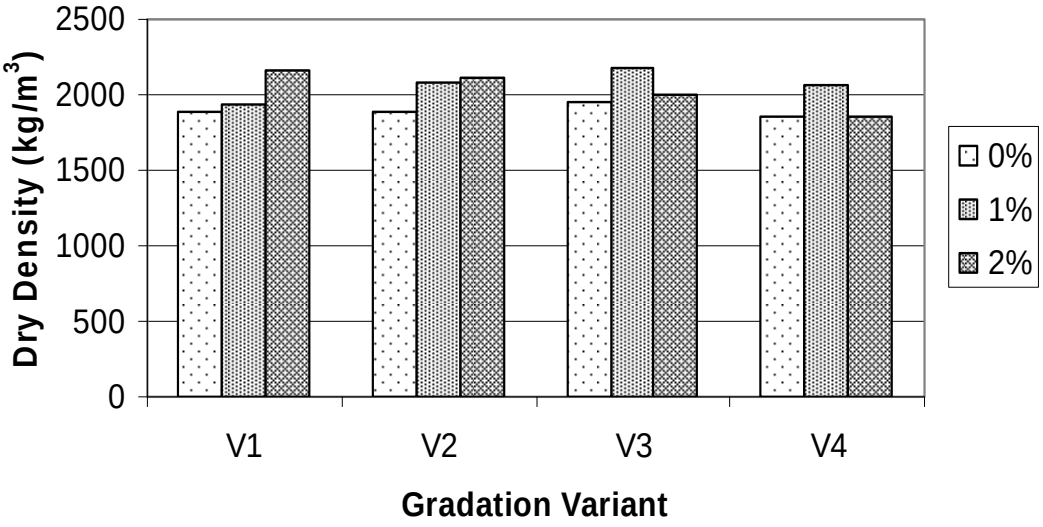

Figure 3-6 Impact of the Variation of Fines Content and Stabilizer Content on the Dry Density of Aggregate Systems Molded at Wet of Optimum Moisture Content

3.3 **Resilient Properties**

The influence of fines and moisture content on the properties of the unbound systems was different than on the stabilized systems. Table 3-4 shows the percentage change in the horizontal and vertical moduli for a given gradation with respect to V1 gradation at the same stabilizer content and moisture condition. For the unbound systems, the resilient moduli of V3 and V4 were either the same or slightly higher than that of V1 under the optimum moisture condition. However, under wet of optimum conditions, the increase in fines content had a detrimental effect on the anisotropic resilient moduli of V3 and V4. The horizontal and vertical moduli of V4 were 87 percent and 70 percent less than their V1 counterparts, respectively. Table 3-4 shows that for the stabilized systems, V3 and V4 had higher resilient moduli than V1 under optimum and wet of optimum conditions. In fact, with 1 percent stabilizer, V3 and V4 significantly outperformed V1 under wet of optimum conditions.

Table 3-7 presents the percentage increase in the moduli of the stabilized systems with respect to the unbound systems at the same fines content. As would be expected, the addition of the stabilizer increased the resilient properties. The high fines content

systems benefited from the stabilizer much more than the low fines content systems. It is interesting to note that V4 stabilized with 1 percent cement significantly outperformed V4 stabilized with 2 percent cement under wet of optimum conditions. During the laboratory experiments, it was noticed that the V4 system with 2 percent cement and in the wet of optimum condition was much more rigid than the other systems, and micro-cracks developed during the test. These cracks reduced the measured resilient properties of this system. As will be discussed later, this behavior was also noticed in the permanent deformation and compression tests. Another observation was that higher resilient modulus values were measured when the molding moisture content was wet of optimum for the stabilized V3 and V4 systems compared to modulus values when the molding moisture was optimum. The excess water is believed to take part in soil-cement strength gain reactions and further enhanced the resilient properties of lightly stabilized aggregate systems.

Table 3-7 Percent Changes in Anisotropic Resilient Moduli of V3 and V4 with Respect to V1 at the Same Conditions

	Unbound				*1% Cement Stabilized*				*2% Cement Stabilized*			
	Optimum		*Wet*		*Optimum*		*Wet*		*Optimum*		*Wet*	
	V3	***V4***	***V3***	***V4***	***V3***	***V4***	***V3***	***V4***	***V3***	***V4***	***V3***	***V4***
Ex	3	19	-48	-87	32	103	62	288	19	51	7	34
Ey	-3	11	-13	-70	43	32	10	85	25	89	3	9

Table 3-8 Percent Changes in Anisotropic Resilient Moduli of Stabilized Systems with Respect to Unbound Systems

	1% Cement Stabilized						*2% Cement Stabilized*					
	Optimum Moisture			*Wet of Optimum*			*Optimum Moisture*			*Wet of Optimum*		
	V1	***V3***	***V4***	***V1***	***V3***	***V4***	***V1***	***V3***	***V4***	***V1***	***V3***	***V4***
Ex	*-10*	*15*	*54*	*20*	*276*	*3442*	*6*	*22*	*35*	*31*	*171*	*1231*
Ey	*-20*	*18*	*-5*	*12*	*42*	*599*	*-17*	*8*	*42*	*6*	*25*	*289*

3.4 **Analysis of Modular Ratios**

A comparison was conducted among the different systems based on the modular ratio (the ratio of horizontal modulus to vertical modulus). As was shown in a number of

earlier studies, the response of a pavement system improves as the anisotropy decreases (increase in the modular value) at a given vertical modulus (Tutumluer, Little et al. 2003). Figure 3-7 shows that an increase in the fines content in the unbound systems at the optimum moisture content resulted in an increase in the modular ratio. Under wet of optimum conditions, however, the modular ratio dramatically decreased as more fines were introduced to the systems (Figure 3-7). When the results in Figures 3-8 and Figure 3-9 are compared to those in Figure 3-7, it can be seen that even a small percentage of stabilizers can increase the modular ratio (reduce the anisotropy) of mixes and improve critical responses in pavement layers.

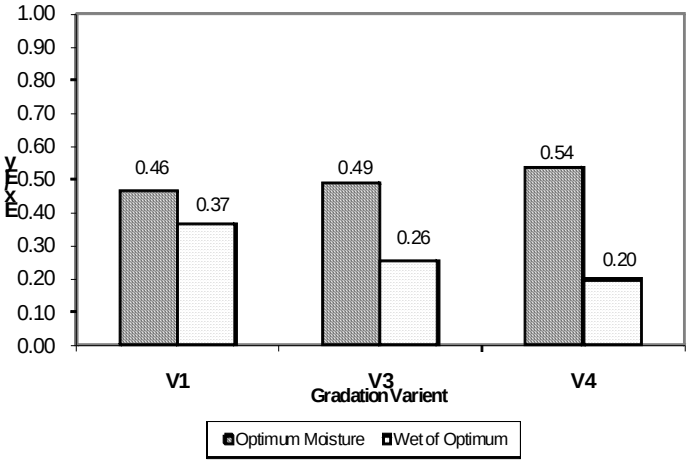

Figure 3-7 Average Modular Ratio for Unbound Aggregate Systems

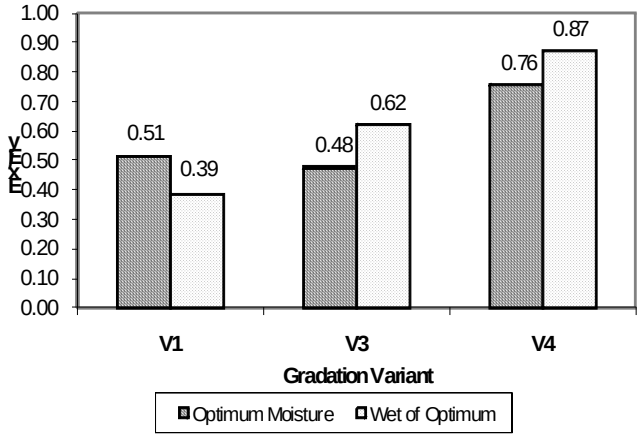

Figure 3-8 Average Modular Ratios for 1 Percent Cement Stabilized Aggregate Systems

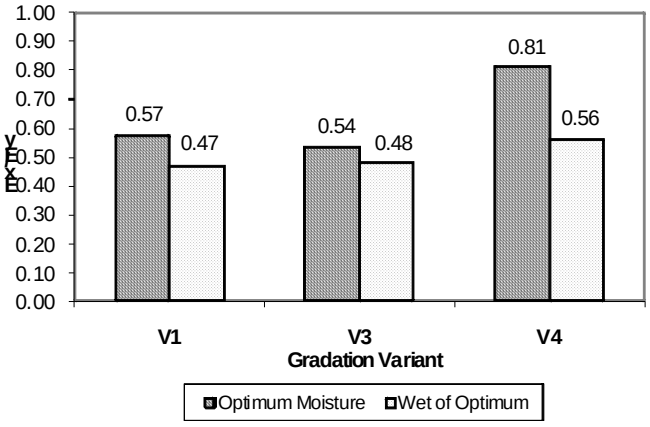

Figure 3-9 Average Modular Ratios for 2 Percent Cement Stabilized Aggregate Systems

CHAPTER 4

TEST RESULTS AND ANALYSIS OF PAVEMENT STRUCTURE

4.1 Permanent Deformation Test Results

The unbound aggregate systems with high fines content (V3 and V4) under wet of optimum conditions reached the maximum strain criterion of 10 percent, and consequently these two tests were terminated before the completion of the 10,000 cycles. The results in Figure 4-1 confirm the deleterious effect of high fines content under wet of optimum conditions on aggregate systems. In the systems with 1 percent Portland cement, adding more fines resulted in a general trend of a lower plastic strain regardless of the moisture content. The same trend was observed for the systems with 2 percent Portland cement at optimum moisture content (Figure 4-1), but it differed for the wet of optimum moisture content since V4 performed poorest at 2 percent stabilizer (Figure 4-2). A plausible explanation for this is that when both the fines content and cement content are high, a more rigid fines matrix results. Such a matrix is likely to be more susceptible to the development of cracks and, therefore, more prone to base layer damage that is reflected in plastic deformation. This finding is in agreement with the analysis of resilient properties.

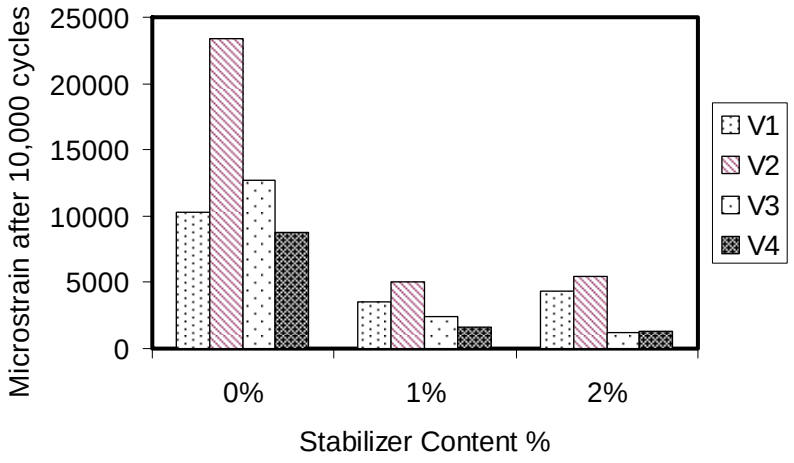

Figure 4-1 Comparison of Permanent Strain at Optimum Moisture Content

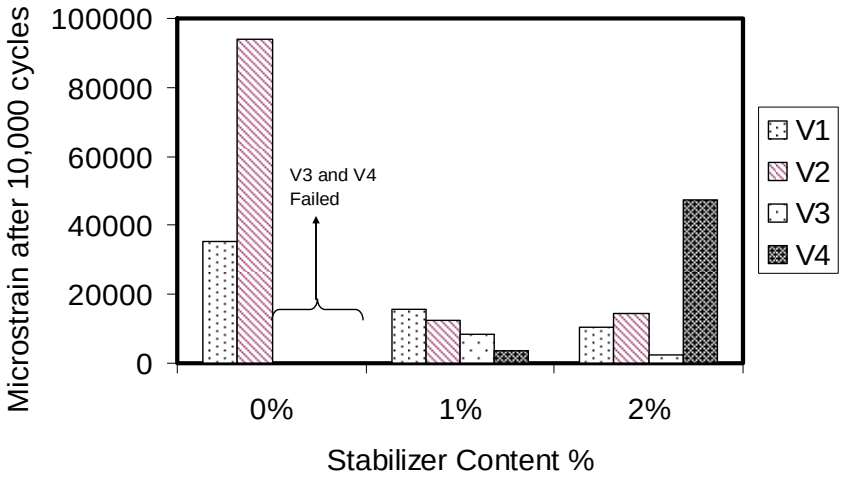

Figure 4-2 Comparison of Permanent Strain at Wet of Optimum Moisture Content

4.2 **Unconfined Compressive Strength**

Unconfined compressive strength tests were performed on specimens compacted at optimum moisture content and then subjected to moisture conditioning. The conditioning time allowed moisture to reach the top of the samples through capillary pores, and not only provided moisture for cement hydration but also provided moisture that impacted the strength and stability of the fines fraction.

The trends in Figure 4-3 demonstrate that stabilizers improved the unconfined compressive strength of the samples tested. In the stabilized systems, V4 typically demonstrated lower strength compared to other gradations. The relationship of strength versus stabilizer content and the fact that the gain in strength for V1, V2, and V3 start to level off after adding 2 percent stabilizer indicate that an optimum point of stabilization exists. This point probably corresponds to a stabilizer-fines content ratio that results in maximum unconfined compressive strength.

Figure 4-3 shows that the highest strength value was achieved in gradation V3 with 2 percent stabilizer. This figure also shows that the unconfined compressive strength

value can be used as a controlling measure to set limits on the amount of fines used in lightly stabilized aggregate systems.

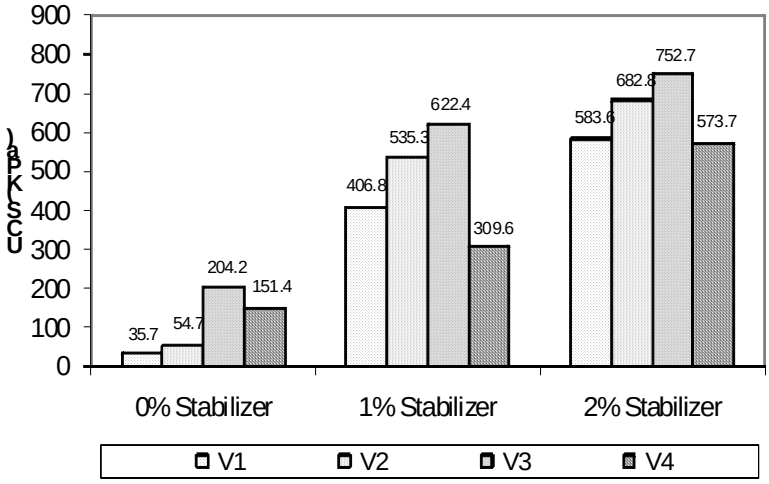

Figure 4-3 Unconfined Compressive Strength for Conditioned Aggregate Systems

Figure 4-4 Shear Banding in 2 Percent Cement Stabilized High Fines System V3

Figure 4-5 Degradation of Particles for Coarse Gradation V1 under Wet Conditions

4.3 **Fines under Light Microscope**

In order to characterize the shape of the fine portion of the gradation chart, materials were examined under the light microscope. Pictures of materials passing sieve #100 (particles smaller than 15 mm) and materials passing sieve #200 (particles smaller than 75 microns) were presented.

Qualitative visual investigation and shape characterization of fine aggregate were performed on the images taken by light microscope. It is evident from these pictures (Figure 4-6 through Figure 4-15) that the crushed siliceous gravel and crushed granite materials have more angular edges compared to limestone materials. Surface asperities in granite material were found to be more distinct compared to limestone materials.

Figure 4-6 Light Microscope Image of Granite Materials (A8) Smaller than 0.15 mm (Passing Sieve #100)

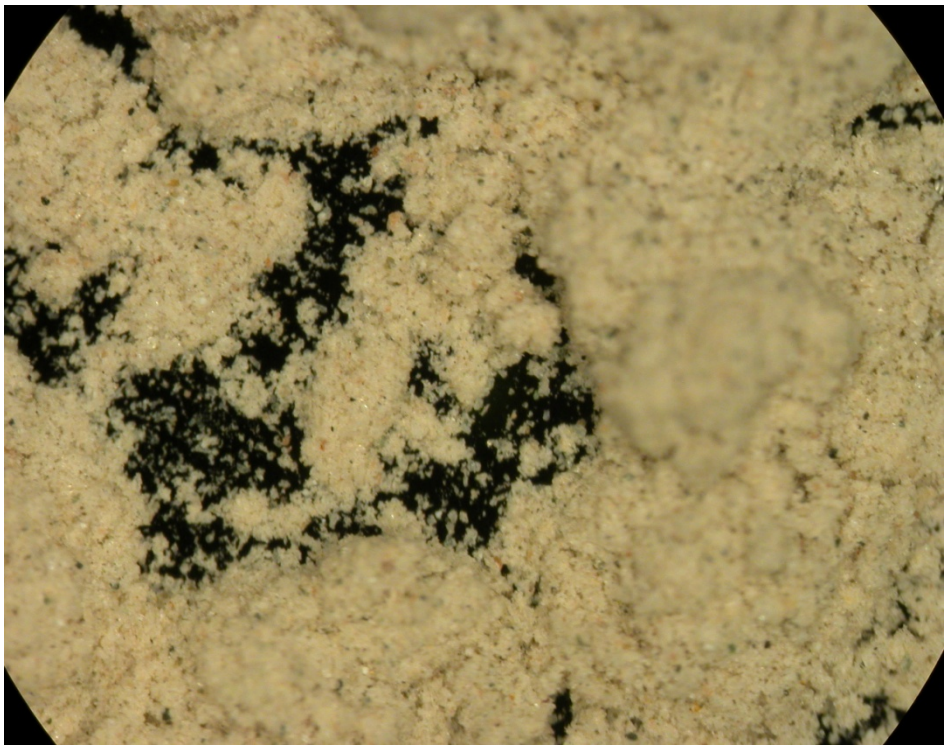

Figure 4-7 Light Microscope Image of Granite Materials (A8) Smaller than 0.075 mm (Passing Sieve #200)

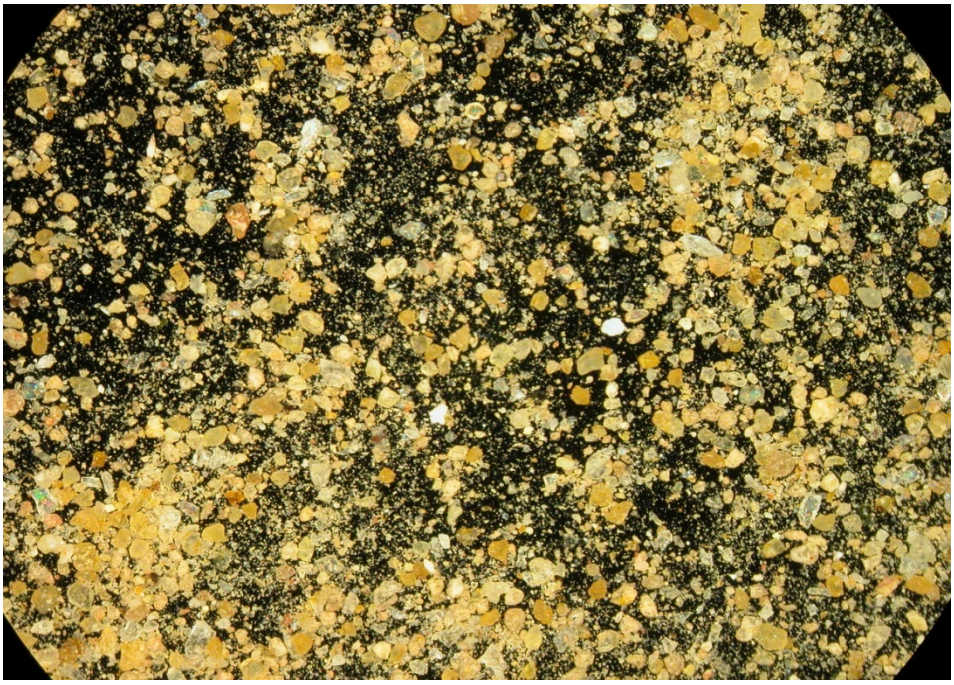

Figure 4-8 Light Microscope Image of Siliceous Gravel (A5) Smaller than 0.15 mm (Passing Sieve #100)

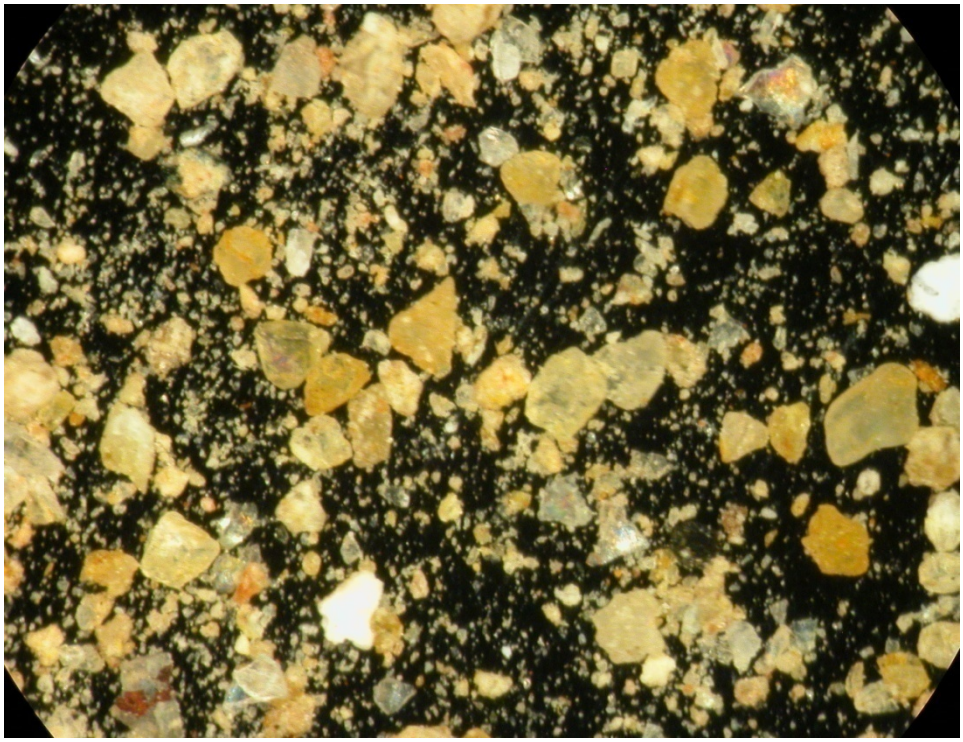

Figure 4-9 Light Microscope Image of Siliceous Gravel (A5) Smaller than 0.075 mm (Passing Sieve #200)

Figure 4-10 Light Microscope Image of Siliceous Gravel (A6) Smaller than 0.15 mm (Passing Sieve #100)

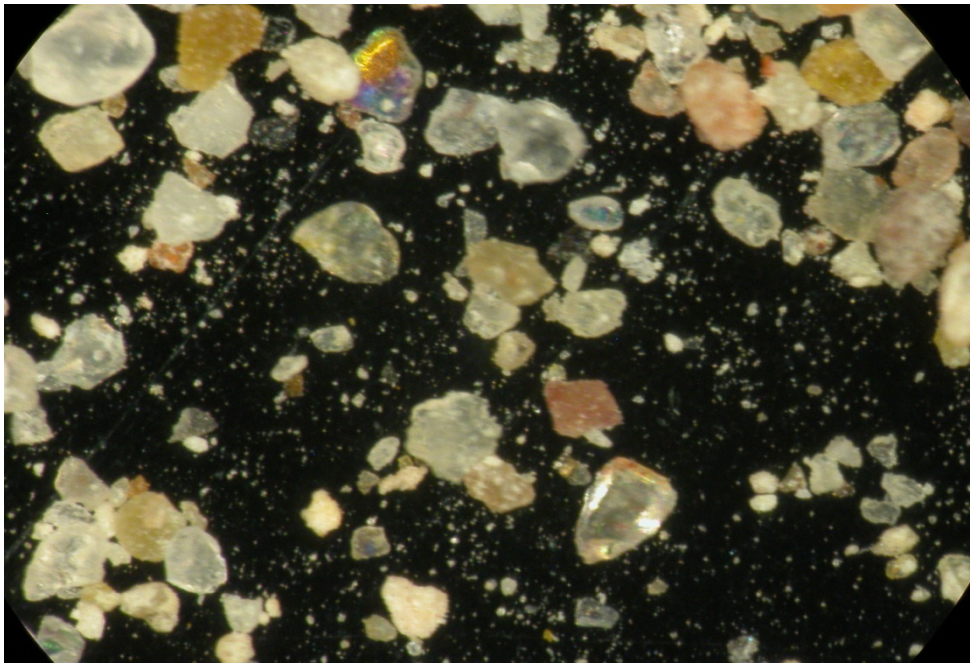

Figure 4-11 Light Microscope Image of Siliceous Gravel (A6) Smaller than 0.075 mm (Passing Sieve #200)

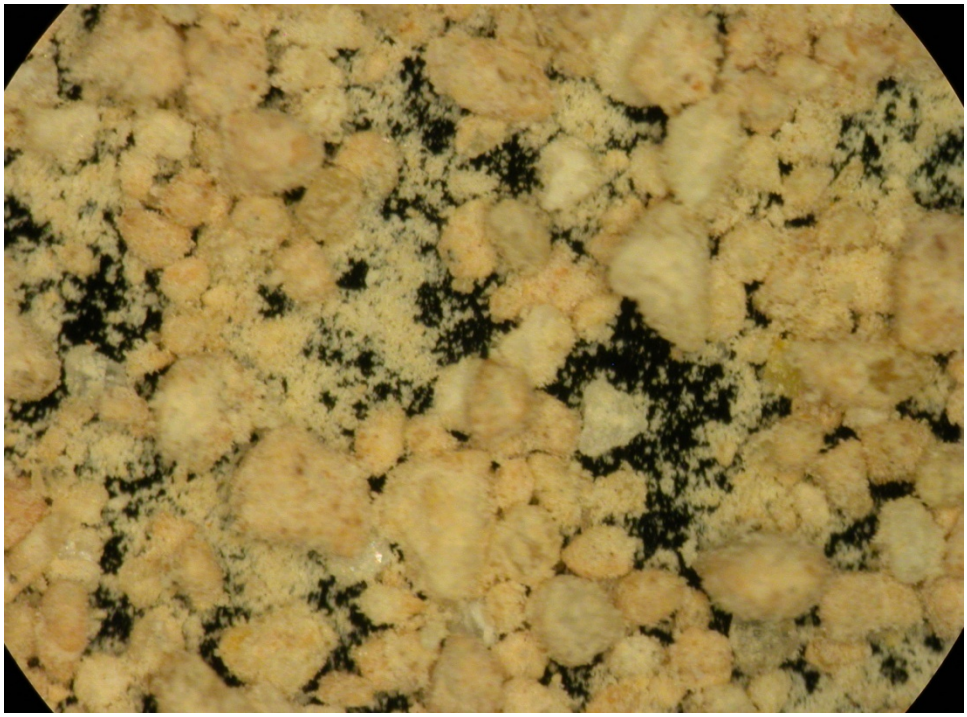

Figure 4-12 Light Microscope Image of Limestone (A7) Smaller than 0.15 mm (Passing Sieve #100)

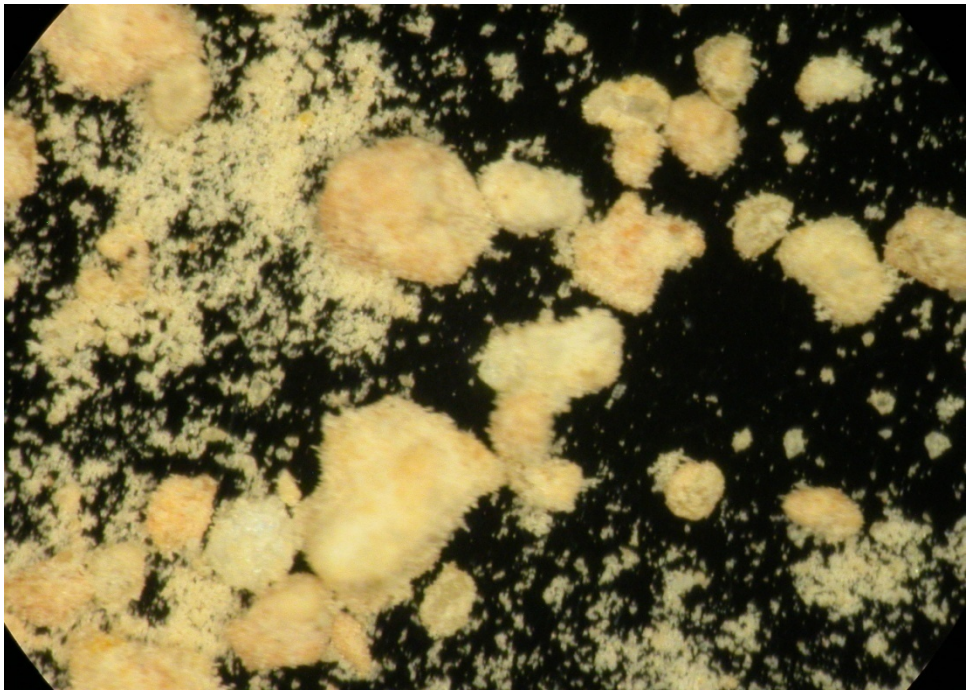

Figure 4-13 Light Microscope Image of Limestone (A7) Smaller than 0.075 mm (Passing Sieve #200)

Figure 4-14 Light Microscope Image of Limestone (A2) Smaller than 0.15 mm (Passing Sieve #100)

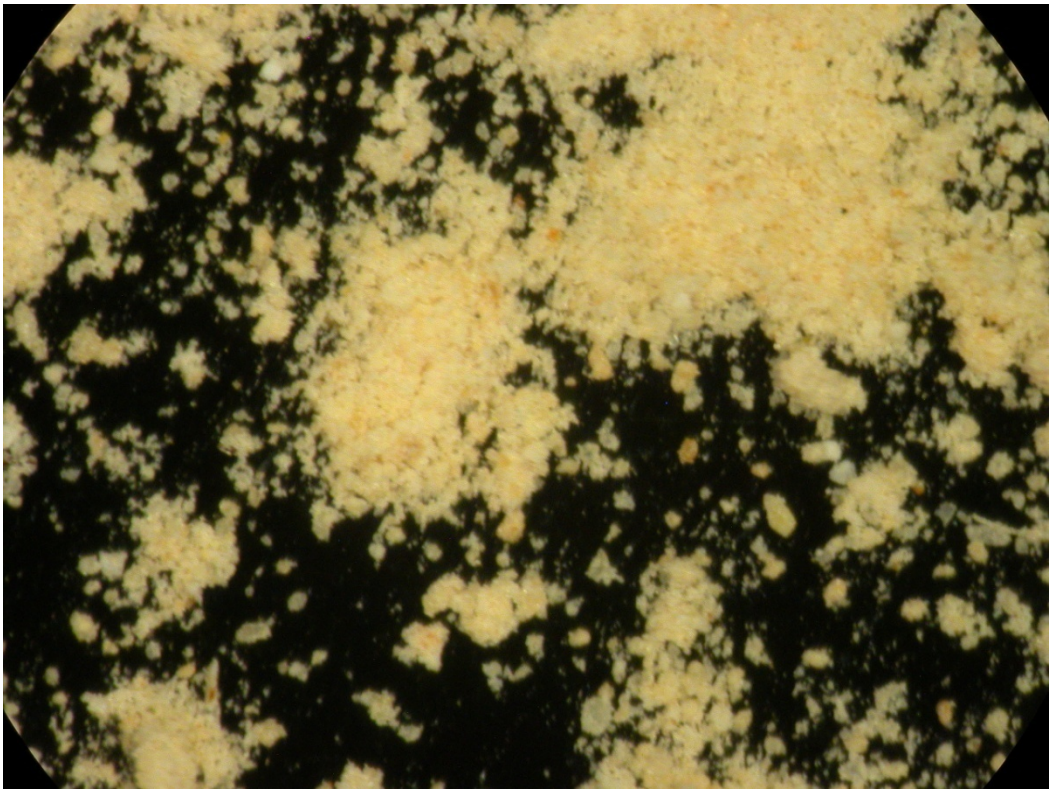

Figure 4-15 Light Microscope Image of Limestone (A2) Smaller than 0.075 mm (Passing Sieve #200)

4.4 Finite Element Analysis

In an anisotropic and nonlinear layer, it is the interaction between the five material properties and stress levels that control the pavement structure response. Therefore, finite element analysis was performed using the TTI-PAVE software to analyze a pavement structure with different unbound and stabilized base layers. TTI-PAVE requires the K parameters in equation 4-1 and m, n, μ, and ν_{xy} where:

$$n = \frac{E_x}{E_y} \qquad m = \frac{G_{xy}}{E_y} \qquad \mu = \frac{\nu_{xx}}{\nu_{xy}} \tag{4-1}$$

ν_{xx} and ν_{xy} are defined as Poisson's ratios in horizontal and vertical directions *(17)*. The analysis was conducted using an axisymmetric finite element mesh with eight node

elements in three layers. A tire pressure of 690 KPa (100 psi) acting on a circular area with a radius of 139.7 mm (5.5 inches) was used in the analysis.

The pavement section consisted of a 150 mm linear isotropic asphalt layer with a modulus of 28,000 MPa (400,000 psi) and a Poisson's ratio of 0.35 resting on a 400 mm thick nonlinear anisotropic aggregate base layer. The base layer was modeled using the material properties of the aggregate systems listed in Table 4-1. The pavement was assumed to be supported by a soft subgrade with a modulus of 41.4 MPa (6000 psi) and Poisson's ratio of 0.45.

Table 4-1 Material Parameters of the Aggregate Systems

Gradation	Stabilizer Content (%)	Moisture Content (%)	$\gamma_{d\ max}$ (kg/cm^3)	$n=E_x/E_y$	$m=G_{xy}/E_y$	ν_{xx}/ν_{xy}
V1 (Wet)	0	7.8	2142	0.37	0.16	1.51
	1	9.9	2181	0.39	0.23	1.79
	2	5.8	2065	0.47	0.29	1.62
V3 (Optimum)	0	7.9	1948	0.49	0.24	2.36
	1	8.1	2119	0.48	0.33	2.49
	2	7.8	2100	0.54	0.39	2.25
V3 (Wet)	0	8.8	2054	0.26	0.2	1.76
	1	10.4	2032	0.62	0.25	1.55
	2	7.7	2102	0.48	0.35	1.56
V4 (Wet)	0	9.3	1851	0.2	0.12	0.77
	1	10.7	2064	0.87	0.34	1.95
	2	9.1	2084	0.56	0.28	2.04

The critical responses, namely vertical strain at the top of the subgrade and horizontal strain at the bottom of the asphalt layer, are tabulated in Table 4-2. As would be expected, there was a clear reduction in critical pavement responses in the stabilized aggregate systems compared to the unbound systems. Table 4-2 shows that V3 with 2 percent stabilizer performed better in samples molded wet of optimum than those molded at optimum moisture conditions. As discussed earlier, this could be the result of additional water in the stabilized system triggering additional cement hydration reactions. Figure 4-16 and Figure 4-17 show a comparison of the critical responses in the wet of optimum condition. For the stabilized systems, the high fines content systems (V3 and V4) performed either similar to or in some cases better than V1. The greatest

improvement was observed for gradation V3 when 2 percent stabilizer was added. As shown in the following section, this finding was in agreement with the results of both the permanent deformation and unconfined compressive strength tests.

Table 4-2 Finite Element Results of Critical Pavement Responses

	Stabilizer(%)	*Strain @ Bottom of Asphalt*	*Strain @ Top of Subgrade*
	0	5.683E-04	1.680E-03
V1 *(Wet)*	*1*	2.613E-04	1.332E-03
	2	2.562E-04	9.113E-04
	0	4.62E-04	1.05E-03
V3 *(Optimum)*	*1*	4.43E-04	1.12E-03
	2	6.70E-04	1.11E-03
	0	8.015E-04	1.890E-03
V3 *(Wet)*	*1*	6.623E-04	1.525E-03
	2	1.546E-04	7.956E-04
	0	9.922E-04	2.205E-03
V4 *(Wet)*	*1*	3.437E-04	1.199E-03
	2	2.195E-04	1.047E-03

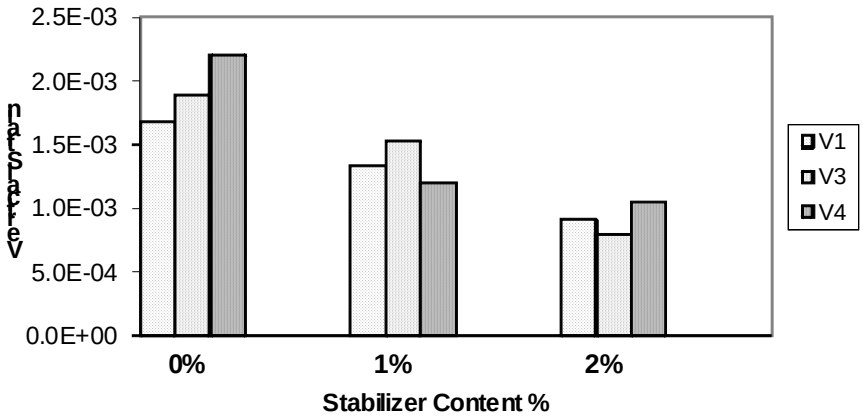

Figure 4-16 Comparison of Vertical Strains at the Top of the Subgrade for a Tested ate Systems ns

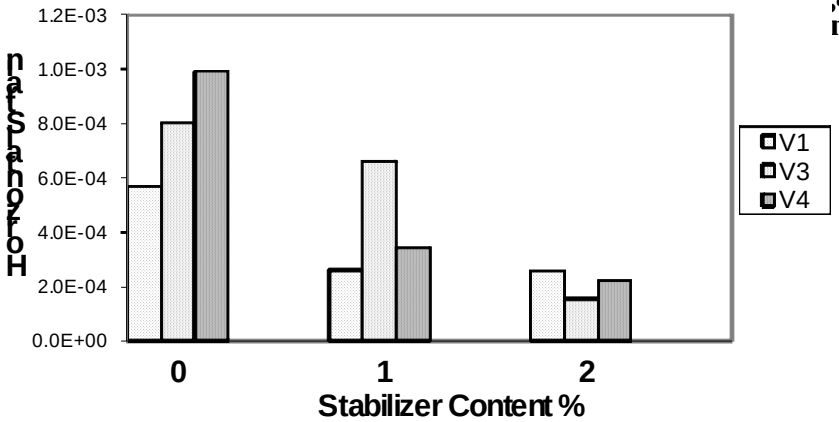

Figure 4-17 Comparison of Tensile Strains at the Bottom of the Asphalt for a Pavement Structure with Different Aggregate Systems Tested at Wet Conditions

CHAPTER 5

PERFORMANCE PREDICTION OF AGGREGATE BASES

5.1 Degree of Nonlinearity

The nonlinear stress-strain behavior of unbound aggregate systems has an important impact on the selection of the design parameters for design of aggregate base layers. It is well established in the literature that the behavior of the aggregate continuum is highly nonlinear and the soil stiffness decays with strain by orders of magnitude. At small strains the magnitude of the stiffness or modulus is large, and at strains close to failure the stiffness or modulus is small and the transition happens in a nonlinear fashion. Several researchers developed constitutive models to capture the nonlinearity of soil stiffness, and many aspects of this are now well understood.

(Atkinson 2000) proposed two measures, namely rigidity (R) and degree of nonlinearity (DN), to quantify the nonlinearity of the stress-strain curve for cohesive soils. The proposed measures of the nonlinearity of stiffness in soils were defined as functions of peak strength and strain at failure calculated/measured using shear wave relations. It should be noted here that the measurement of soil stiffness must be performed over the full range of the stress path to determine soil stiffness at small strains and large deformations. This information is imperative in the mechanistic design of pavement foundations.

Figure 5-1 illustrates a typical stiffness-strain relationship for soils. As demonstrated in this figure, stiffness of soils is relatively large at small strains, and it decays as the strain increases. At small strains (shear strains smaller than 0.001 percent) the response behavior of soil can be considered linear. In the small strain region the stiffness of the unbound aggregate system is constant and is referred to as initial modulus, or E_{max}, in the soil mechanics literature. The stiffness of modulus value calculated for this region can be

considered the non damaged stiffness or modulus. However, the stiffness decays in a nonlinear fashion as the aggregate system is subjected to a more demanding stress path. This will induce non-recoverable plastic strains; the stiffness or the modulus calculated for this region of the stress-strain curve is referred to as damaged stiffness or damaged modulus.

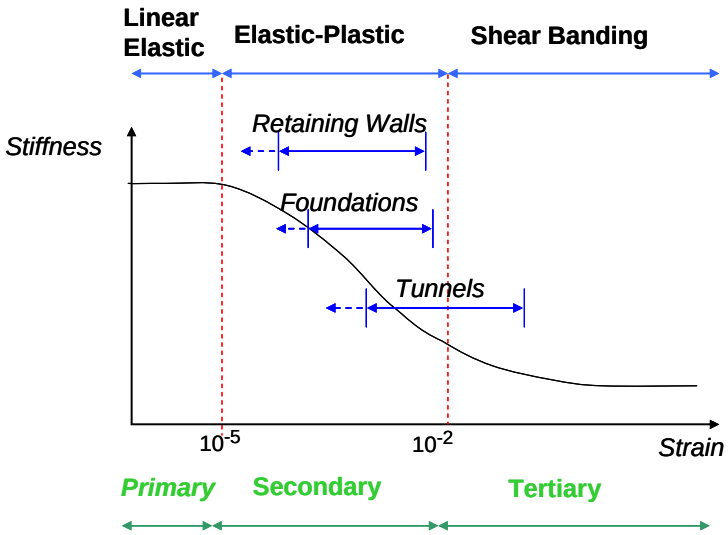

Figure 5-1 Characteristic Stress-Strain Behavior of Soils

In characterizing the nonlinearity of response in unbound aggregate systems, it is necessary to consider both stiffness and strain at failure and the relationship between them. A triaxial device is commonly used to measure the intermediate to large strain stiffness using various ranges of stress paths. Dynamic methods such as shear wave propagation techniques and resonant columns were used to calculate the small strain behavior of soils. Dynamic methods will be discussed later in this chapter.

Figure 5-2 shows typical inflicted strains due to application of different stress protocols in the lab. This figure emphasizes the importance of the testing method and testing protocol in determination of the design stiffness. The NCHRP 1-28A protocol is the most demanding loading protocol. This protocol imposes stress states up to the development of damage in the system and initiation of shear band. AASHTO T-307 and ICAR loading

protocols are mainly focused on the range of stress states (and strains) imposed by traffic load. Stiffness measured using shear wave propagation techniques is primarily out of the range of strains imposed by traffic loads and results in very high stiffness values.

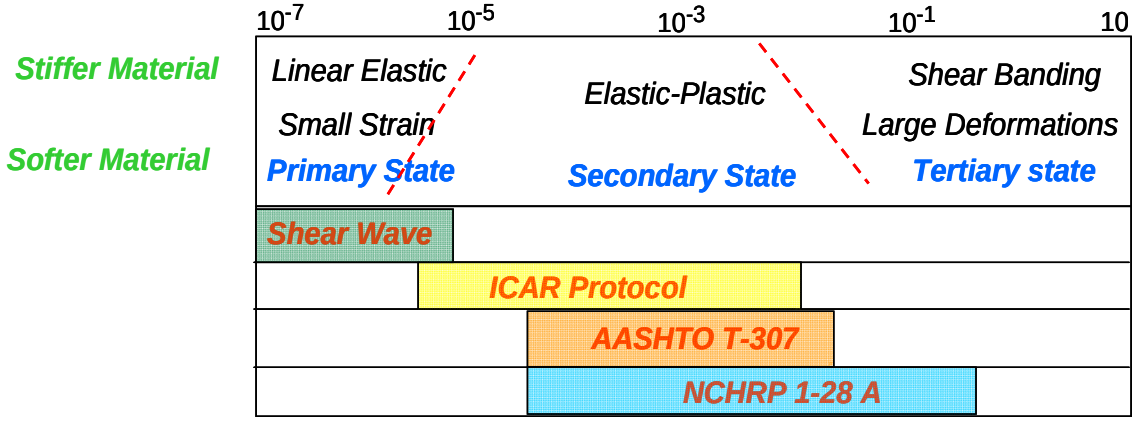

Figure 5-2 Strain Level and Prescribed Stress Protocols in the Lab

5.2 Measures of Nonlinearity

Stiffness nonlinearity is a common and important feature of compacted granular materials. This property has usually been represented by the nonlinear stress dependent relationship between resilient modulus and axial strain. In order to quantify the nonlinearity of different aggregate systems, (Atkinson and Sallfors 1991) proposed two measures for capturing the nonlinearity of geomaterials:

- rigidity (r) and
- degree of nonlinearity (m).

Figure 5-3 illustrates the typical stress strain behavior of two geomaterials. The stiff system, which shows less nonlinearity, is represented by a red curve, and the softer aggregate system with a larger nonlinear range is presented in blue. In this figure q is the deviator stress that is the difference between axial and radial stresses, and ε_f is the strain at the onset of failure. E_o is the initial modulus that is the tangent modulus in the initial stage of applying the stress path. In Figure 5-3, q_f denotes the deviatoric stress at failure.

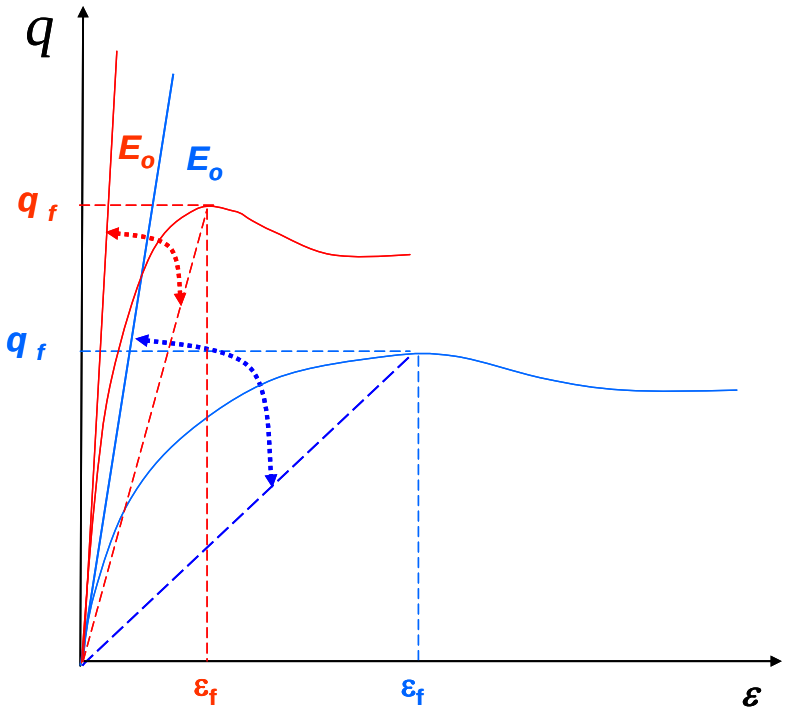

Figure 5-3 Typical Stress-Strain Behavior for Stiff and Soft Aggregate System

Rigidity is defined as the ratio of modulus to the strength of the soil continuum:

$$r = \frac{E_o}{q_f} = \frac{1}{\varepsilon_o} \tag{5-1}$$

It should be noted here that the reference strain (ε_r) is simply defined from the rigidity and is not a strain at any characteristic point during loading.

The ratio of stiffness (characterized by modulus in this approach) to strength appears in many geotechnical models. An example of this is solutions for cavity expansion developed by Vesic. He presented an argument on the validity of the stiffness-strength ratio as the criterion that determines the ductility or brittleness of materials. He later defined the ratio of shear modulus (G_{xy}) to undrained strength (S_u) in the triaxial test as the rigidity index for geomaterials (Vesic 1970).

In order to characterize the nonlinearity of the geomaterials, two measures were defined. Atkinson used the ratio of strains as a characterizer of the nonlinearity of soil samples, as presented in equation 5-2:

$$m_1 = \frac{\varepsilon_f}{\varepsilon_r} \tag{5-2}$$

where ε_f is the strain at which the material fails as illustrated in Figure 5-3. Researchers also used another measure, the ratio of deviatoric stresses at failure (q_f), to maximum deviatoric stress in the linear portion of the stress-strain curve.

$$m_2 = \frac{q_f}{q_r} \tag{5-3}$$

5.3 **Analysis of the Degree of Nonlinearity**

Figure 5-4 through Figure 5-6 show the level of nonlinearity results for stabilized and lightly stabilized aggregate systems. Figure 5-4 shows the variation of the degree of nonlinearity based on the deviatoric stress ratios in the aggregate samples. Figure 5-4 clearly shows that using (q_f/q_r) resulted in a physically meaningful plot of the data. As illustrated in Figure 5-4, adding fines to the mix in unbound systems (0 percent stabilizer) resulted in a significant increase in the degree of nonlinearity of the aggregate samples.

Figure 5-4 also shows the drastic reduction in the level of nonlinearity of the aggregate systems when small percentages of stabilizer were added to the system. Figure 5-5 and Figure 5-6 are another representation of the analysis of nonlinearity in aggregate samples. Figure 5-4 illustrates the change in the degree of nonlinearity characterized by (q_f/q_r) as the stabilizer content increases in the mix. A nonlinearity characterizer ($\varepsilon f/\varepsilon r$) was used to study the impact of stabilizer content on the reduction of the level of nonlinearity in the

aggregate blends. Both figures show that the aggregate samples with low percentages of stabilizer were significantly less nonlinear than their unbound counterparts.

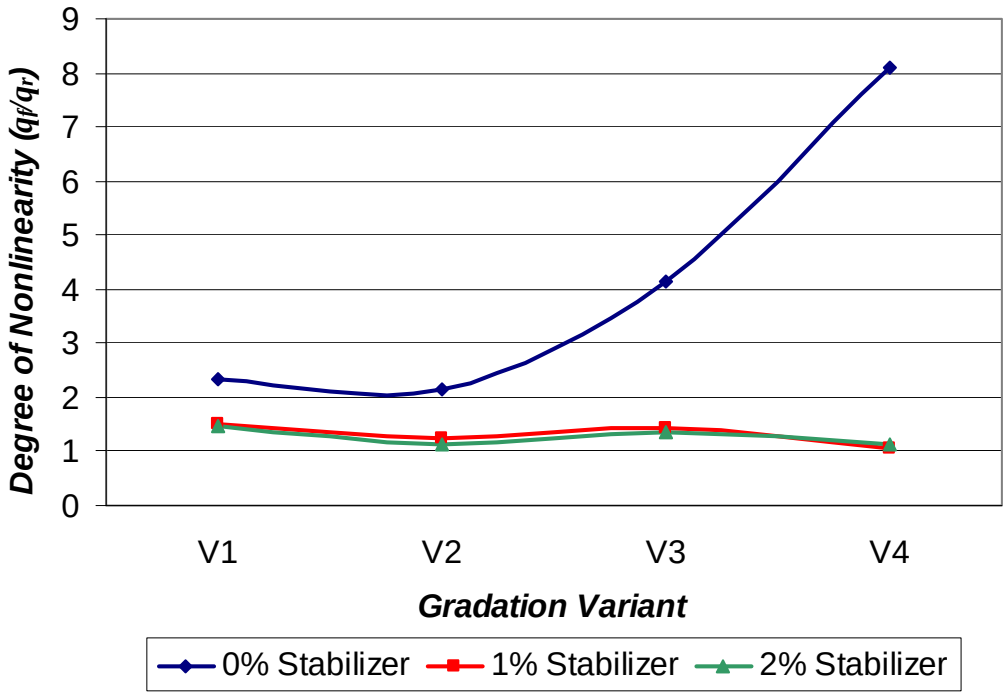

Figure 5-4 Variation of the Degree of Nonlinearity Based on Deviatoric Stress Ratios

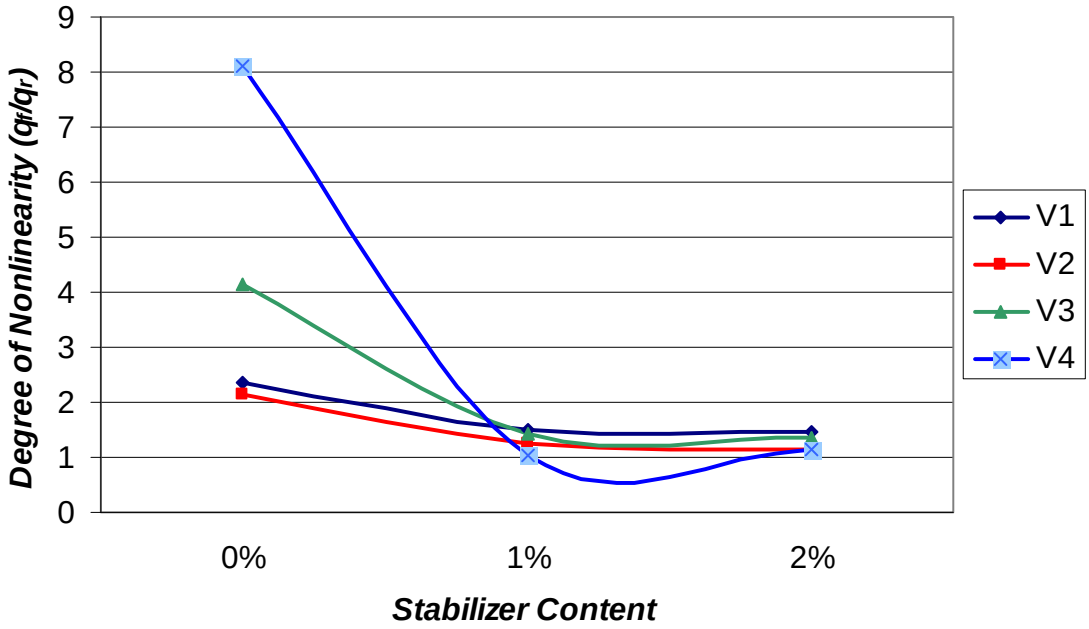

Figure 5-5 Analysis of the Degree of Nonlinearity Based on Deviatoric Stress Ratios

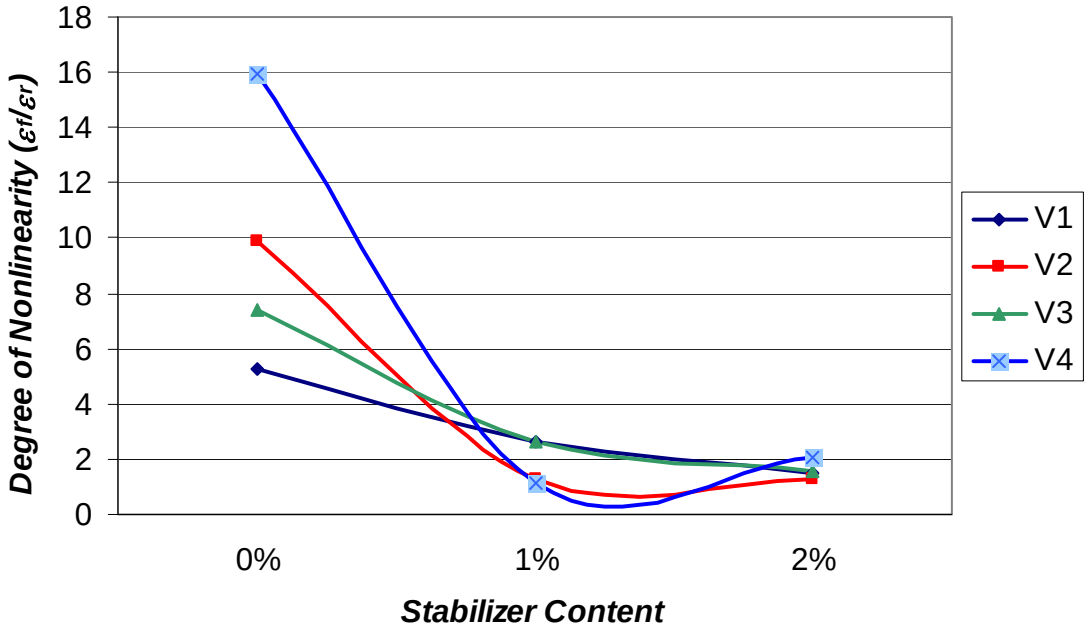

Figure 5-6 Analysis of the Degree of Nonlinearity Based on Strain Ratios

5.4 **Structural Stability of the Aggregate Systems**

Figure 5-7 shows the representation of the state of stresses acting on the body of a soil specimen using the Mohr circle. The Mohr-Coulomb failure envelope shown in Figure 5-7 defines the boundary below which the combination of stress states does not cause significant plastic deformation in the body of the material and the continuum stays stable. According to the Mohr-Coulomb theory, the strength of the body is determined by cohesion and friction between the particles of soil and can be found from:

$$\tau_{max} = c + \sigma_n \tan \phi \qquad (5\text{-}4)$$

where:

- $_{max}$ = the maximum shear stress at the failure,
- σ_n = the normal stress acting on the failure plane and makes an angle of $\theta = (\pi/4 + \phi/2)$ with the horizontal plane, and
- c and ϕ = cohesion and angle of internal friction, respectively

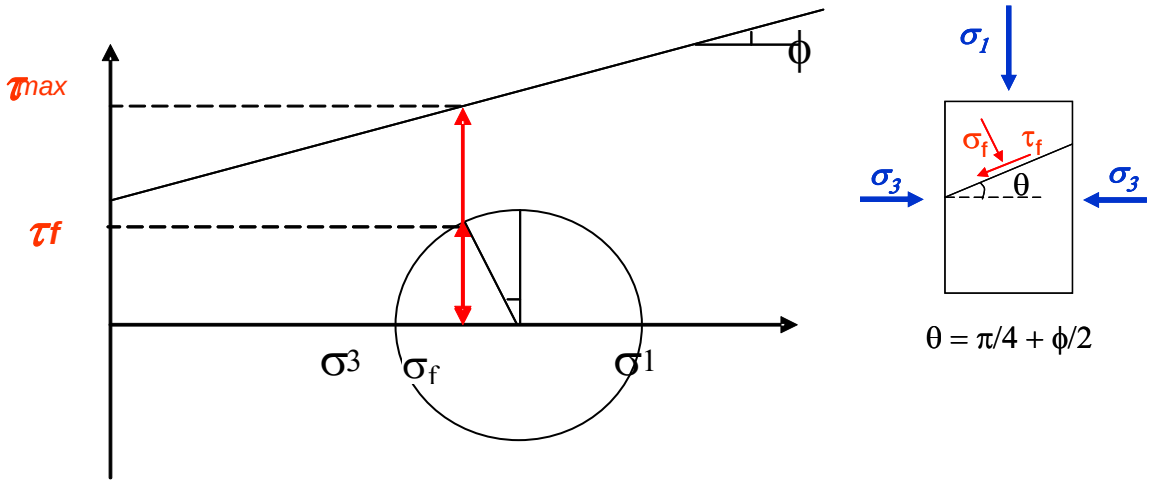

Figure 5-7 Illustration of the Concept of the Shear Stress Ratio Using the Mohr Circle

As illustrated in Figure 5-7, at any arbitrary stress state a shear stress ratio of (τ_f/τ_{max}) defines the fraction of shear strength τ_{max} that is acting on the failure plane due to the prescribed stress states. This concept was primarily developed (Thompson 1990) for NCHRP 1-26 for the stability control of subgrade soils. He used the ratio of deviatoric stress to unconfined compressive strength of the subgrade soils (σ_d/UCCS) as a measure of performance for subgrades. Thompson also showed that a reasonable relationship exists between field rutting data and the shear strength ratio of subgrade. He concluded that there is a limiting value of (σ_d/UCCS), above which the subgrade is prone to permanent deformation. He suggested a limiting value for the stress ratios to be below 0.4 to ensure the stability of subgrades under traffic loads.

Based on the same rationale, researchers used the ratio of maximum octahedral shear stress $(\tau_{oct})_{max}$ calculated in the base layer and unconfined compressive strength of the soil cement aggregate systems as the performance indicator in this study, as seen in equation 5-5. The value of $(\tau_{oct})_{max}$ was calculated using anisotropic solutions and used as input to equation 5-5.

$$Shear\ Strength\ Ratio\ (SSR) = \frac{Octahedral\ Shear\ Stress\ at\ Top\ of\ Base\ Layer}{Unconfined\ Compressive\ Strength} \qquad (5\text{-}5)$$

It should be noted here that the shear stresses calculated due to traffic loads found from the anisotropic solutions are typically higher than shear stresses found from the isotropic solutions, which ultimately results in higher stress ratios. As mentioned earlier in this chapter, higher shear stress ratios correspond to situations in which the stability of the pavement is in jeopardy and the base layer is prone to develop non-recoverable plastic deformations.

5.5 **Analysis of Shear Stresses in the Base Layer**

Shear stress was calculated using TTI-PAVE throughout the base layer for a single wheel with 100 psi tire pressure. The base material was considered to be stress sensitive and cross anisotropic for calculating the shear stresses in the base layer. The unconfined compressive strength (UCCS) was determined from laboratory testing following the ASTM D2166 procedure. The test results for the unconfined compressive strengths were presented in chapter three of this report. The shear strength ratios were calculated using equation 5-5. The contour plots for the shear stresses in the base layer are presented in Figure 5-8 through Figure 5-10. The plots are for the controlled system using gradation V1 (with 5 percent passing sieve #200) at the optimum moisture state. Figure 5-8 shows that maximum shear stress occurred at the top of the base layer and aligned at the edge of the tire. The magnitude of shear stress was calculated to be 17.3 psi for the controlled system with gradation V1.

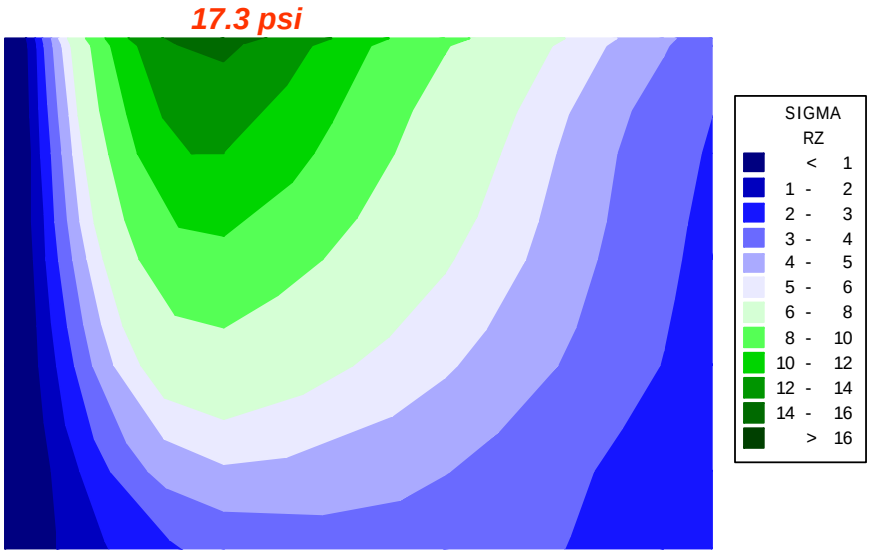

Figure 5-8 Shear Stress Distribution in the Base Layer for Controlled System (V1)

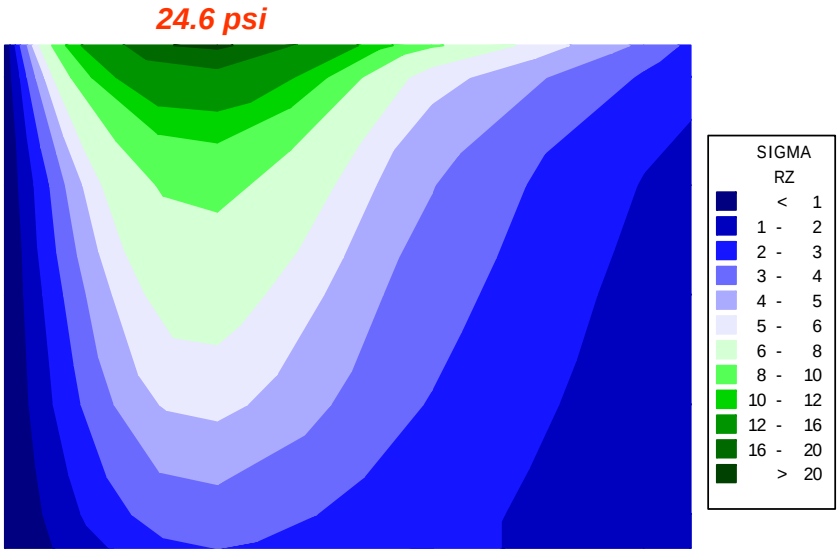

Figure 5-9 Shear Stress Distributions in the Base Layer for Unstabilized (V3) System under Wet Conditions

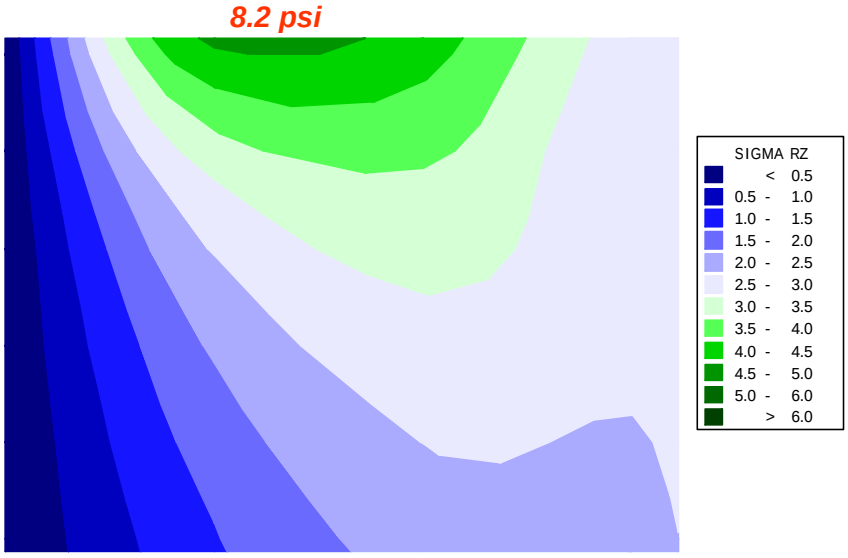

Figure 5-10 Shear Stress Distribution in the Base Layer for 2 Percent Cement Stabilized System (V3) under Wet Conditions

Figure 5-9 and Figure 5-10 show the shear stresses developed in the base layer for a three-layer pavement system with 4 inches of 500,000 psi asphalt modulus paved over a subgrade with a modulus of 6000 psi. Gradation V3 with 30 percent passing sieve #40 and 15 percent passing sieve #200 was selected to show the impact of low levels of stabilization in elevated saturation levels. Figure 5-9 shows the shear stress distribution in the base layer for gradation V3 under wet conditions. Maximum shear stress developed in the aggregate layer was 24.6 psi. A comparison between the controlled system with gradation V1 at optimum moisture states with high fines system V3 under wet conditions shows a significant increase in the shear stresses developed in the base layer. The maximum anisotropic shear stress developed in the base layer in the high fines system was found to be 29 percent higher than the controlled system. This agrees with expectations for witnessing higher shear stresses when the fines content increases in the unbound aggregate base layer.

Figure 5-10 shows the shear stresses developed in the base layer for the system with light stabilization and high fines content at elevated saturation levels. Anisotropic material properties for gradation V3 were used as inputs to a finite element program to calculate shear stresses and produce the shear stress contour plot presented in Figure 5-10. Maximum shear stress was calculated to be 8.2 psi for this variant. The results clearly illustrate a significant reduction in the shear stresses developed in the base layer when 2 percent type I cement was added to the high fine aggregate system. The maximum shear stress was reduced by 200 percent at the top of the subgrade for the 2 percent cement stabilized V3 system when compared to the same unstabilized system V3. The lightly stabilized high fines gradation (V3) has performed better in terms of shear stresses developed in the base layer. The results indicate that the maximum shear stress was reduced by about 110 percent when the high fines but stabilized system was used in lieu of the controlled system V1. Shear stresses calculated in the stabilized system indicate that light stabilization of the high fines system significantly outperforms the controlled system and the high fines system.

5.6 **Analysis of Shear Strength Ratios**

Anisotropic solutions were used to calculate the octahedral shear stresses in the base layer. Later, the shear strength ratios were calculated using equation 5-5. Figure 5-11 and Figure 5-12 illustrate the distribution of the shear strength ratios developed in the pavement layer. As mentioned earlier in the previous section of this chapter, maximum shear stresses—and consequently maximum shear strength ratios—were found to be aligned with the edge of the tire and occur at the top of the base layer.

Figure 5-11 presents the contour plot for the distribution of shear strength ratios for high fines system (gradation V3 with 30 percent passing sieve #40 and 15 percent passing sieve #200) under wet conditions. Similar to the nonlinear distribution of shear stresses shown in Figures 5-8 through 5-10, shear strength ratios also vary in nonlinear fashion throughout the aggregate layer. The highest shear strength value calculated for this combination was 0.43 at the top of the aggregate layer.

Figure 5-11 illustrates the distribution of shear strength ratios in the base layer for a three-layer pavement system. Anisotropic material properties for 2 percent cement stabilized gradation V3 were used as inputs to the nonlinear and cross-anisotropic finite element program to calculate the octahedral shear stresses throughout the base layer. The maximum shear strength ratio was calculated to occur at the top of the base layer aligned with the edge of the tire. The magnitude of the shear strength in this variant was calculated to be 0.12.

As discussed earlier in this chapter, lower shear strength values are synonymous with more stable pavement systems. In other words, aggregate bases with lower shear strength values are less prone to develop plastic deformations and rut under traffic loads. A comparison between the two cases discussed earlier shows that adding 2 percent cement to the high fine aggregate system V3 under wet conditions resulted in a significant reduction (about 258 percent) in the shear strength ratio. Considering the argument presented by (Thompson 1992) in NCHRP 1-26 that lower shear strength ratios correspond to lower rut potential in the pavement, the performance of the lightly

stabilized high fines systems will be superior to their unbound counterparts, and these systems can be considered for potential use in highway systems.

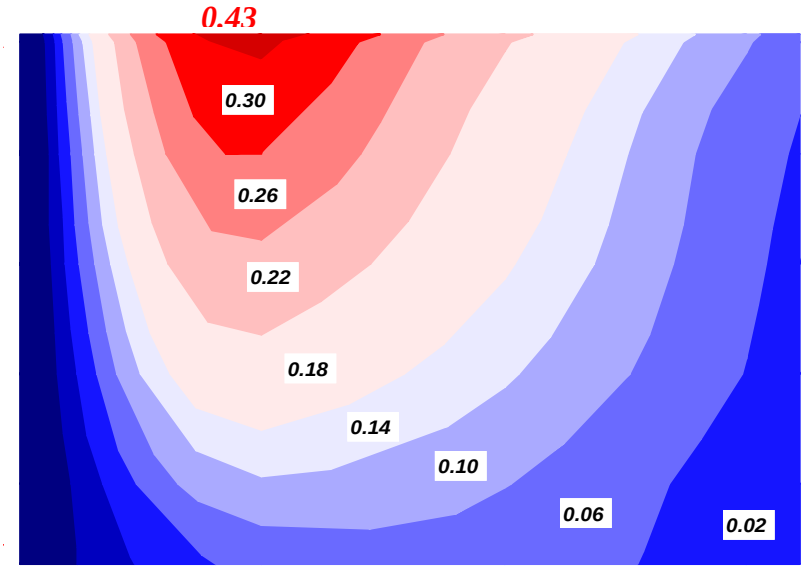

Figure 5-11 Shear Strength Ratios for High Fines System V3 under Wet Conditions

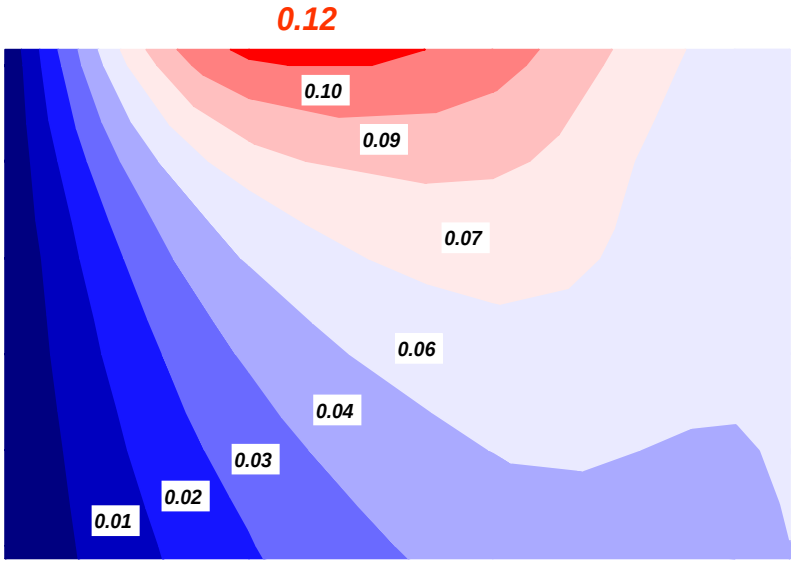

Figure 5-12 Shear Strength Ratios for 2 Percent Cement Stabilized High Fines System V3 under Wet Conditions

5.7 **Plastic Deformation at the Surface**

In another effort to evaluate the performance of stabilized and unstabilized high fine aggregate systems, anisotropic solutions were used to calculate the plastic strains at the top of the pavement surface.

Figure 5-13 shows the plastic deformations at the top of the asphalt layer for several variants. The anisotropic material properties of gradation V1 (with 5 percent passing sieve #200) at optimum moisture content were considered as the control system. These material properties were used as inputs to a nonlinear, stress-sensitive, and cross-anisotropic finite element program (TTI-PAVE) to calculate the deformation at the surface. The results presented in Figure 5-13 indicate that unbound high fines content aggregate systems V3 and V4 resulted in higher plastic strains at the top of the asphalt layer as expected. The surface deformations were more pronounced for gradation V4 with 40 percent passing sieve #40 and 20 percent passing sieve #200.

Figure 5-13 illustrates that the 2 percent cement stabilized high fines systems at elevated saturation levels performed better than the controlled system in terms of surface deformations. An important observation in this figure is the fact that 2 percent cement stabilized gradation V3 performed better than 2 percent cement stabilized gradation V4. This suggests that there exists a limiting value of fines in the mix, above which the performance deteriorates. This observation agrees with the unconfined compressive strength and repeated load permanent deformation test results discussed earlier.

Figure 5-14 shows the percentage improvement of deterioration of performance based on the surface deflection calculated using nonlinear, stress-sensitive, and anisotropic solutions. In this figure, gradation V1 with no stabilizer at the optimum moisture state was considered as a reference system, and the surface deformation of other variants were compared to this system. The results show that when 2 percent type I cement is added to the control system V1, the deformation at the surface is reduced by 32 percent. The rate of improvement is much more pronounced for high fines systems upon stabilization.

Figure 5-14 shows that when 2 percent stabilizer is added to the high fines systems V3 and V4, the deformation at the surface decreases by 43.5 percent and 33.7 percent, respectively. On the other hand, unstabilized high fines systems resulted in loss of performance in terms of plastic deformation at the top of the asphalt layer. Figure 5-14 illustrates that when the fines content increases from 5 percent in the control system to 15 percent and 20 percent in gradations V3 and V4, respectively, deformation on the top of the pavement increases by 15.1 percent and 116 percent, respectively. These results agree with the unconfined compressive strength test and repeated load permanent deformation test presented earlier in this report.

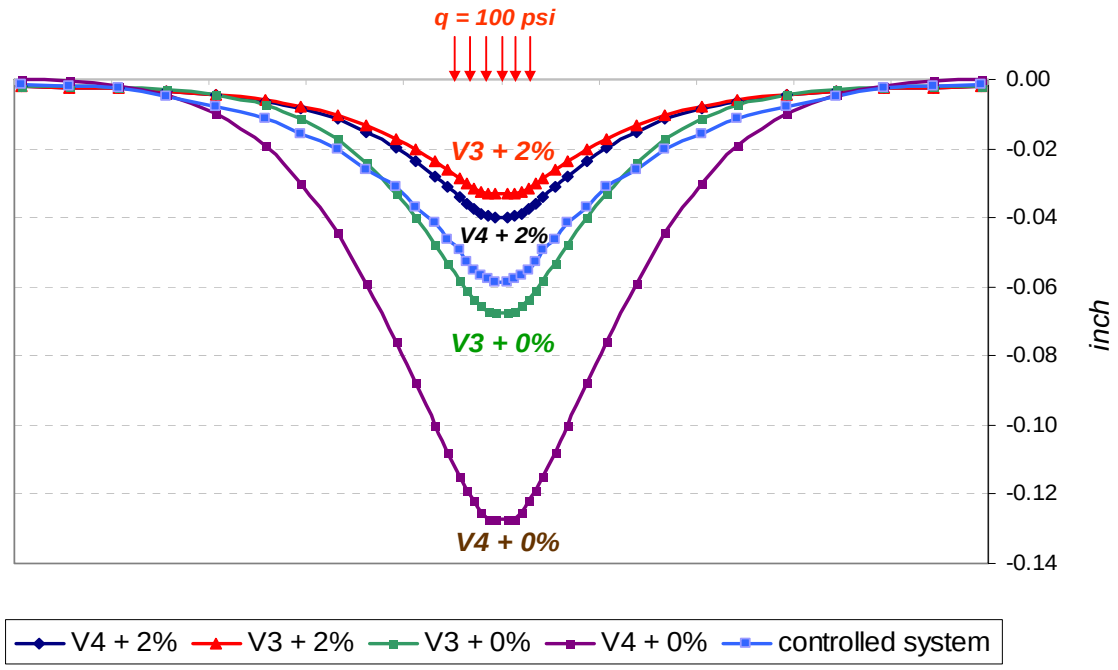

Figure 5-13 Finite Element Predictions of Plastic Deformation on the Surface

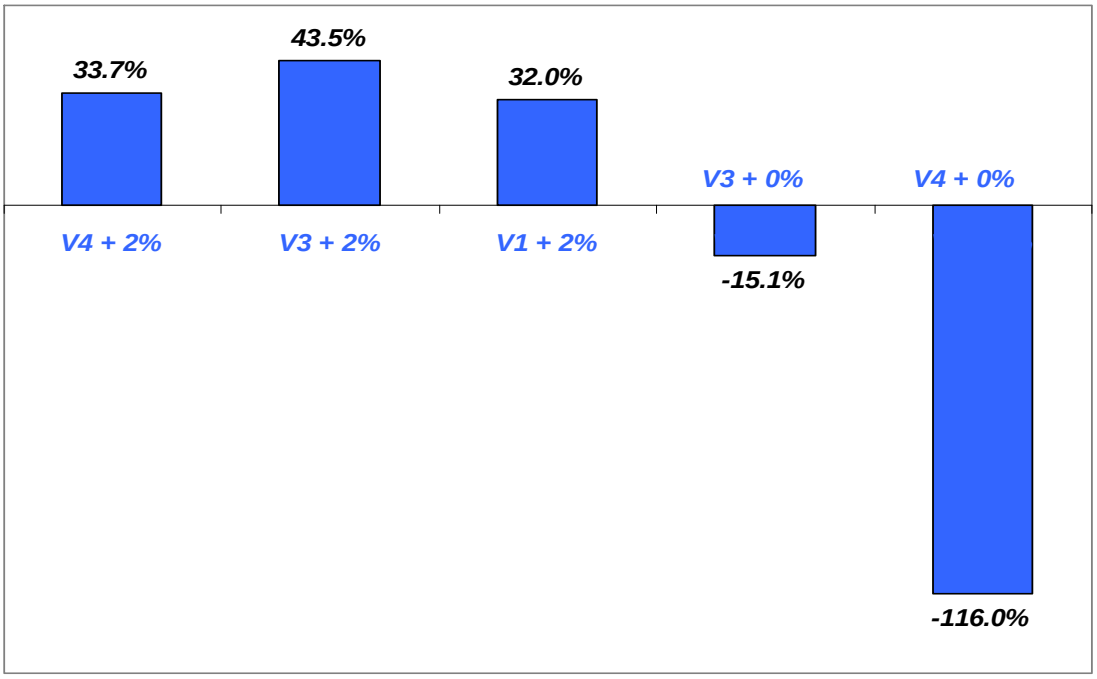

Figure 5-14 Percent Improvement (Loss) of Performance in Terms of Decrease (Increase) of Plastic Deformation at the Pavement Surface

REFERENCES

Ahn, N. and D. W. Fowler (1999). Past and Current Fines Research. ICAR (International Center for Aggregate Research) 7th annual Symposium, University of Texas at Austin.

Atkinson, J. (2000). "Nonlinear Soil Stiffness in Routine Design." Geotechnique **50**(5): 487-588.

Atkinson, J. and Sallfors (1991). Experimental Determination of Stress-Strain-Time Characteristics in laboratory and In-Situ Tests. 10th Europian Conference onSoil mechanics and Foundation Engineering, Florance, Italy.

Bateman, A. (2003). Dufferin implements cost effective improvements, breaks with tradition. Aggregates & Roadbuilding Magazine.

Bolen, W. P., R. S. Kalyoncu, et al. (1996). U.S. Geological Survey Minerals Yearbook **1:** 940

Brown, D. (1996). Use of waste fines as backfill material. ICAR (International Center for Aggregate Research) 4rth Annual Symposium

D. Rockliff (1996). Low-grade quarry products, reclaimed aggregates and inert wastes - their use in unbound mixtures for road pavements. *Waste Management*. **16:** pp 83-85.

De Rezende, L. R. and J. C. De Carvalho (2003). "The use of quarry waste in pavement construction." Resources, Conservation and Recycling **39**(1): 91-105.

Gray, J. E. (1962). Characteristics of Graded Coarse Aggregates Determined by Triaxial Tests. Alexandria, VA., Engineering Research Bulletin.

Hudson, W. R., D. N. Little, et al. (1997). *An Investigation of the Status of By-Product Fines in the USA* . Research Report for Project "Uses of By-Product Fines. The University of Texas-Austin.

Machemehl, C. (1996). The future of the aggregate industry. 4th Annual Aggregates Symposium. Atlanta, GA, International Center for Aggregate Research.

Manning, D. and J. Vetterlein (2004). Exploitation and Use of Quarry Fines. Manchester, UK, MIRO Mineral Solutions.

Parker, F. (1996). Crushed stone fines for mechanically stabilized earth walls. 4th annual symposium, International Center for Aggregate Research, University of texas at Austin.

Seberras, D. (2000). "Little John" improves productivity, reduces fines. Aggregates & Roadbuilding Magazine.

Simonsen, E., V. C. Janoo, et al. (2002). "Resilient Properties of Unbound Road Materials during Seasonal Frost Conditions." Journal of Cold Regions Engineering **16**(1): 28-50.

Thadkamalla, B. G. and K. P. George. (1995). "Characterization of Subgrade Soils at Simulated Field Moisture." *Transportation Research Record 1481*, Journal of Transportation Research Board, National Research Council, Washington, D.C.: pp. 21-28.

Thompson, M. R. (1990). "NCHRP 1-26: Calibrated Mechanistic Structural Analysis Procedures for Pavements, Volume II - Appendices, Prepared for the National Cooperative Highway Research Program, Transporation Research Program." Transportation Research Board, National Research Council,Washington, D.C.

Thompson, M. R. (1992). "NCHRP 1-26: Calibrated Mechanistic Structural Analysis Procedures for Pavements Phase 2, Volume II - Appendices, Prepared for the National Cooperative Highway Research Program, Transporation Research Program, ." Transportation Research Board, National Research Council, Washington, D.C. .

Touahamia, M., V. Sivakumar, et al. (2002). "Shear strength of reinforced-recycled material." Construction and Building Materials **16**(6): 331-339.

Tutumluer, E., D. Little, et al. (2003). "Validated Model for Predicting Field Performance of Aggregate Base Courses." Transportation Research Record: Journal of the Transportation Research Board **1837**(-1): 41-49.

Tutumluer, E. and U. Seyhan (1999). "Laboratory Determination of Anisotropic Aggregate Resilient Moduli Using an Innovative Test Device." Transportation Research Record: Journal of the Transportation Research Board **1687**(-1): 13-21.

Vesic, A. S. (1970). "Expansion of cavities in infinite soil mass." Journal of Geotechnical Engineering, ASCE **98**(SM3): 265-290.

Wood, S. A. (1995). Pond fines: Waste not. Want not-industry commitment to by-product fines. 3rd Annual Aggregate Symposium, International center for Aggregate Research.

APPENDIX A

TABLE OF MATERIAL PROPERTIES

Table A-1 Anisotropic Material Properties for Gradation V1 at Optimum Moisture Content and with 0 Percent Stabilizer

σ_1 (kPa)	σ_3 (kPa)	I (kPa)	τ_{oct} (kPa)	E_x (kPa)	E_y (kPa)	G_{xy} (kPa)	G_{xx} (kPa)	ν_{xy}	ν_{xx}
50	25	100	11.79	407999	890773	275735	159715	0.06	0.28
70	40	150	14.14	604957	1006382	358166	284996	0.07	0.06
130	60	250	33.00	586732	1260794	382653	257851	0.08	0.14
150	70	290	37.71	655110	1534296	501672	253912	0.10	0.29
220	120	460	47.14	874550	1585566	554187	395713	0.07	0.11
250	140	530	51.85	926828	1777538	621547	429220	0.09	0.08
250	120	490	61.28	782687	2403273	635593	253537	0.26	0.54
250	105	460	68.35	799426	2170726	609756	287506	0.18	0.39

Table A-2 Anisotropic Material Properties for Gradation V2 at Optimum Moisture Content and with 0 Percent Stabilizer

σ_1 (kPa)	σ_3 (kPa)	I (kPa)	τ_{oct} (kPa)	E_x (kPa)	E_y (kPa)	G_{xy} (kPa)	G_{xx} (kPa)	ν_{xy}	ν_{xx}
40	25	90	7.07	54772	254237	37552	22071	0.09	0.24
50	25	100	11.79	54800	327355	37074	22548	0.08	0.22
70	40	150	14.14	136783	430444	103591	58355	0.12	0.17
130	60	250	33.00	212539	632105	145773	94609	0.08	0.12
150	70	290	37.71	273992	934316	235849	100946	0.14	0.36
170	100	370	33.00	262203	995824	259516	94036	0.17	0.39
220	120	460	47.14	345603	1062527	279503	140149	0.14	0.23
250	140	530	51.85	378461	1310265	313370	140675	0.18	0.35
250	120	490	61.28	376636	1460939	361156	129749	0.17	0.45
250	105	460	68.35	392732	1587452	319602	143293	0.20	0.37

Table A-3 Anisotropic Material Properties for Gradation V3 at Optimum Moisture Content and with 0 Percent Stabilizer

σ_1 (kPa)	σ_3 (kPa)	I (kPa)	τ_{oct} (kPa)	E_x (kPa)	E_y (kPa)	G_{xy} (kPa)	G_{xx} (kPa)	ν_{xy}	ν_{xx}
50	25	100	11.79	282735	999478	235110	108391	0.03	0.30
130	60	250	33.00	658052	1209481	390625	319481	0.06	0.03
150	70	290	37.71	757207	1451523	513699	298408	0.11	0.27
250	140	530	51.85	897040	1615723	554187	404778	0.12	0.11
250	120	490	61.28	1140855	2014781	568182	490644	0.15	0.16
250	105	460	68.35	877957	1867575	558313	361331	0.15	0.21

Table A-4 Anisotropic Material Properties for Gradation V4 at Optimum Moisture Content and with 0 Percent Stabilizer

σ_1 (kPa)	σ_3 (kPa)	I (kPa)	τ_{oct} (kPa)	E_x (kPa)	E_y (kPa)	G_{xy} (kPa)	G_{xx} (kPa)	ν_{xy}	ν_{xx}
40	25	90	7.07	506078	975507	342466	188231	0.04	0.34
50	25	100	11.79	680883	1151239	423968	274879	0.13	0.24
70	40	150	14.14	793574	1209709	465839	341594	0.09	0.16
130	60	250	33.00	856913	1448135	553506	328353	0.13	0.30
170	100	370	33.00	962594	1707956	614754	392228	0.14	0.23
220	120	460	47.14	830130	2037554	655977	290660	0.19	0.43
250	140	530	51.85	1275576	2979479	698758	574886	0.25	0.11
250	120	490	61.28	800970	2476130	673653	244088	0.31	0.64

Table A-5 Anisotropic Material Properties for Gradation V1 at Wet of Optimum Moisture State and with 0 Percent Stabilizer

σ_1 (kPa)	σ_3 (kPa)	I (kPa)	τ_{oct} (kPa)	E_x (kPa)	E_y (kPa)	G_{xy} (kPa)	G_{xx} (kPa)	ν_{xy}	ν_{xx}
40	25	90	7.07	72962	467291	52588	30067	0.15	0.21
50	25	100	11.79	66942	387321	61779	26685	0.07	0.25
70	40	150	14.14	158958	406815	125839	83535	0.11	-0.05
130	60	250	33.00	183730	651261	141777	70366	0.13	0.31
150	70	290	37.71	288403	792113	227964	106333	0.14	0.36
170	100	370	33.00	334617	713910	234742	141449	0.14	0.18
220	120	460	47.14	409054	745146	257437	191455	0.08	0.07
250	140	530	51.85	490193	886248	303235	224969	0.10	0.09
250	120	490	61.28	435410	1392751	296834	167094	0.21	0.30
250	105	460	68.35	418325	1012693	284810	182941	0.10	0.14

Table A-6 Anisotropic Material Properties for Gradation V2 at Wet of Optimum Moisture State and with 0 Percent Stabilizer

σ_1 (kPa)	σ_3 (kPa)	I (kPa)	τ_{oct} (kPa)	E_x (kPa)	E_y (kPa)	G_{xy} (kPa)	G_{xx} (kPa)	ν_{xy}	ν_{xx}
40	25	90	7.07	200143	416710	98307	97072	0.05	0.03
50	25	100	11.79	130036	470040	96154	49476	0.08	0.31
70	40	150	14.14	269782	474421	153689	143201	0.07	-0.06
130	60	250	33.00	227430	637046	146628	92389	0.11	0.23
150	70	290	37.71	301509	881960	226244	109708	0.13	0.37
170	100	370	33.00	375139	779960	261780	162614	0.10	0.15
220	120	460	47.14	425723	876274	268176	188988	0.09	0.13
250	140	530	51.85	486107	1025855	326560	218042	0.09	0.11
250	120	490	61.28	351126	1461822	300000	115565	0.24	0.52
250	105	460	68.35	368657	1072980	258621	159897	0.09	0.15

Table A-7 Anisotropic Material Properties for Gradation V3 at Wet of Optimum Moisture State and with 0 Percent Stabilizer

σ_1 (kPa)	σ_3 (kPa)	I (kPa)	τ_{oct} (kPa)	E_x (kPa)	E_y (kPa)	G_{xy} (kPa)	G_{xx} (kPa)	ν_{xy}	ν_{xx}
50	25	100	11.79	55278	328066	48860	21188	0.07	0.30
70	40	150	14.14	108024	287415	77399	57678	0.07	-0.06
130	60	250	33.00	96401	456156	73638	37888	0.11	0.27
150	70	290	37.71	136949	632217	117925	51762	0.10	0.32
170	100	370	33.00	181633	508474	143678	87660	0.10	0.04
220	120	460	47.14	202045	582179	141598	101413	0.08	0.00
250	140	530	51.85	258238	695468	181598	131577	0.09	-0.02
250	120	490	61.28	157029	1173503	156467	54509	0.20	0.44
250	105	460	68.35	136347	1158008	139147	46841	0.17	0.46

Table A-8 Anisotropic Material Properties for Gradation V1 at Optimum Moisture Content and with 1 Percent Stabilizer

σ_1 (kPa)	σ_3 (kPa)	I (kPa)	τ_{oct} (kPa)	E_x (kPa)	E_y (kPa)	G_{xy} (kPa)	G_{xx} (kPa)	ν_{xy}	ν_{xx}
40	25	90	7.07	304847	681939	154776	130901	0.11	0.16
50	25	100	11.79	342322	820023	187032	56475	0.11	2.03
70	40	150	14.14	458693	777046	274725	208341	0.09	0.10
130	60	250	33.00	544205	968725	321888	258786	0.06	0.05
150	70	290	37.71	643812	1295099	431034	254109	0.12	0.27
170	100	370	33.00	714515	1313584	464396	302214	0.12	0.18
220	120	460	47.14	843767	1296535	479744	418307	0.06	0.01
250	140	530	51.85	922733	1526293	548780	457096	0.08	0.01
250	120	490	61.28	799461	2122272	548780	276792	0.23	0.44
250	105	460	68.35	785377	1855399	533175	312232	0.14	0.26

Table A-9 Anisotropic Material Properties for Gradation V2 at Optimum Moisture Content and with 1 Percent Stabilizer

σ_1 (kPa)	σ_3 (kPa)	I (kPa)	τ_{oct} (kPa)	E_x (kPa)	E_y (kPa)	G_{xy} (kPa)	G_{xx} (kPa)	ν_{xy}	ν_{xx}
50	25	100	11.79	619215	666686	292740	297654	0.05	0.04
70	40	150	14.14	1015995	768792	389004	435227	0.14	0.17
130	60	250	33.00	962041	1077504	423729	344950	0.25	0.39
150	70	290	37.71	1251790	1020801	510031	551415	0.08	0.14
170	100	370	33.00	1348871	1056840	528914	617447	0.09	0.09
220	120	460	47.14	1343106	1174157	556931	649303	0.09	0.03
250	140	530	51.85	1295081	1273401	608108	626437	0.07	0.03
250	120	490	61.28	1057167	1723858	609756	327120	0.33	0.62
250	105	460	68.35	1148131	1623244	614754	390644	0.24	0.47

Table A-10 Anisotropic Material Properties for Gradation V3 at Optimum Moisture Content and with 1 Percent Stabilizer

σ_1 (kPa)	σ_3 (kPa)	I (kPa)	τ_{oct} (kPa)	E_x (kPa)	E_y (kPa)	G_{xy} (kPa)	G_{xx} (kPa)	ν_{xy}	ν_{xx}
40	25	90	7.07	528203	879104	295119	214035	0.10	0.23
50	25	100	11.79	316946	1023836	258621	117660	0.03	0.35
70	40	150	14.14	632468	1305290	431530	252224	0.12	0.25
130	60	250	33.00	778930	1510339	530035	340161	0.07	0.14
150	70	290	37.71	997202	1725886	627615	441029	0.07	0.13
170	100	370	33.00	1012444	1790483	665779	438313	0.07	0.15
220	120	460	47.14	1074580	2001887	732899	458164	0.08	0.17
250	140	530	51.85	1025617	2428077	800712	396509	0.13	0.29
250	120	490	61.28	875993	2784545	815217	262394	0.26	0.67
250	105	460	68.35	1134939	2597932	812274	406530	0.17	0.40

Table A-11 Anisotropic Material Properties for Gradation V4 at Optimum Moisture Content and with 1 Percent Stabilizer

σ_1 (kPa)	σ_3 (kPa)	I (kPa)	τ_{oct} (kPa)	E_x (kPa)	E_y (kPa)	G_{xy} (kPa)	G_{xx} (kPa)	ν_{xy}	ν_{xx}
50	25	100	11.79	209922	1069731	417362	57089	0.02	0.84
70	40	150	14.14	1130948	1129021	513347	534791	0.07	0.06
130	60	250	33.00	1297191	1524061	632378	489100	0.14	0.33
150	70	290	37.71	1418332	1663261	810373	539831	0.11	0.31
170	100	370	33.00	1178796	1826704	768443	441036	0.11	0.34
220	120	460	47.14	1276425	1878665	803571	577303	0.06	0.11
250	140	530	51.85	1211750	1948413	786713	576703	0.04	0.05
250	120	490	61.28	1743137	1932056	842697	937933	0.03	0.07
250	105	460	68.35	2169333	2018993	916497	1068483	0.06	0.02

Table A-12 Anisotropic Material Properties for Gradation V1 at Wet of Optimum Moisture State and with 1 Percent Stabilizer

σ_1 (kPa)	σ_3 (kPa)	I (kPa)	τ_{oct} (kPa)	E_x (kPa)	E_y (kPa)	G_{xy} (kPa)	G_{xx} (kPa)	ν_{xy}	ν_{xx}
40	25	90	7.07	82239	274590	68683	36221	0.14	0.14
50	25	100	11.79	104268	381624	88235	44905	0.13	0.16
70	40	150	14.14	150097	516374	124792	54228	0.18	0.38
130	60	250	33.00	255484	758751	178147	91377	0.15	0.40
150	70	290	37.71	372933	914505	269300	138598	0.15	0.35
170	100	370	33.00	365429	821428	269300	146501	0.16	0.25
220	120	460	47.14	467796	976808	304465	203513	0.11	0.15
250	140	530	51.85	572000	1169904	372517	252614	0.13	0.13
250	120	490	61.28	539828	1216003	362319	212786	0.13	0.27
250	105	460	68.35	516822	1297108	362903	199890	0.14	0.29

Table A-13 Anisotropic Material Properties for Gradation V2 at Wet of Optimum Moisture State and with 1 Percent Stabilizer

σ_1 (kPa)	σ_3 (kPa)	I (kPa)	τ_{oct} (kPa)	E_x (kPa)	E_y (kPa)	G_{xy} (kPa)	G_{xx} (kPa)	ν_{xy}	ν_{xx}
70	40	150	14.14	196789	623668	156250	65420	0.19	0.50
130	60	250	33.00	244571	809577	181818	90465	0.13	0.35
150	70	290	37.71	348563	954529	278293	130582	0.14	0.33
170	100	370	33.00	356315	888702	279851	150976	0.15	0.18
220	120	460	47.14	432137	1040738	304878	194791	0.10	0.11
250	140	530	51.85	479221	1183800	358852	215356	0.08	0.11
250	120	490	61.28	473564	1319736	363489	196021	0.11	0.21
250	105	460	68.35	486772	1347931	367647	201206	0.11	0.21

Table A-14 Anisotropic Material Properties for Gradation V3 at Wet of Optimum Moisture State and with 1 Percent Stabilizer

σ_1 (kPa)	σ_3 (kPa)	I (kPa)	τ_{oct} (kPa)	E_x (kPa)	E_y (kPa)	G_{xy} (kPa)	G_{xx} (kPa)	ν_{xy}	ν_{xx}
40	25	90	7.07	226158	437020	110698	107786	0.08	0.05
70	40	150	14.14	382245	642307	234375	153818	0.15	0.24
130	60	250	33.00	404385	790550	246305	153448	0.14	0.32
150	70	290	37.71	601111	1016625	366748	227937	0.13	0.32
170	100	370	33.00	684292	933550	373134	293750	0.13	0.16
220	120	460	47.14	715003	1000918	384615	328208	0.09	0.09
250	140	530	51.85	767216	1116992	417440	353979	0.10	0.08
250	120	490	61.28	764414	1180050	425331	324840	0.12	0.18
250	105	460	68.35	718482	1162057	405405	302426	0.11	0.19

Table A-15 Anisotropic Material Properties for Gradation V4 at Wet of Optimum Moisture State and with 1 Percent Stabilizer

σ_1 (kPa)	σ_3 (kPa)	I (kPa)	τ_{oct} (kPa)	E_x (kPa)	E_y (kPa)	G_{xy} (kPa)	G_{xx} (kPa)	ν_{xy}	ν_{xx}
50	25	100	11.79	187211	956502	328947	52492	0.02	0.78
70	40	150	14.14	1604654	1086057	543085	760530	0.20	0.05
130	60	250	33.00	1172671	1295674	563698	523836	0.08	0.12
150	70	290	37.71	1908010	1422082	742942	1097072	0.02	-0.13
170	100	370	33.00	1200422	1642764	711913	473949	0.09	0.27
220	120	460	47.14	1683841	1660659	755034	1024119	0.03	-0.18
250	140	530	51.85	1135025	1992203	778547	458207	0.10	0.24
250	120	490	61.28	1434526	1890862	815217	666907	0.05	0.08
250	105	460	68.35	1654365	1947381	835499	782112	0.07	0.06

Table A-16 Anisotropic Material Properties for Gradation V1 at Optimum Moisture Content and with 2 Percent Stabilizer

σ_1 (kPa)	σ_3 (kPa)	I (kPa)	τ_{oct} (kPa)	E_x (kPa)	E_y (kPa)	G_{xy} (kPa)	G_{xx} (kPa)	ν_{xy}	ν_{xx}
40	25	90	7.07	492561	767923	253300	198970	0.15	0.24
50	25	100	11.79	223342	855143	225904	77842	0.03	0.43
70	40	150	14.14	597390	859463	327941	313661	0.06	-0.05
130	60	250	33.00	663564	1120585	391645	319188	0.06	0.04
150	70	290	37.71	828225	1342073	515464	367732	0.07	0.13
220	120	460	47.14	1022087	1420501	559701	536876	0.05	-0.05
250	140	530	51.85	1098606	1568120	625000	564847	0.05	-0.03
250	120	490	61.28	860615	2193155	613079	290246	0.24	0.48
250	105	460	68.35	953928	1727227	601604	407754	0.10	0.17

Table A-17 Anisotropic Material Properties for Gradation V2 at Optimum Moisture Content and with 2 Percent Stabilizer

σ_1 (kPa)	σ_3 (kPa)	I (kPa)	τ_{oct} (kPa)	E_x (kPa)	E_y (kPa)	G_{xy} (kPa)	G_{xx} (kPa)	ν_{xy}	ν_{xx}
40	25	90	7.07	50300	141000	37800	23955	0.02	0.05
50	25	100	11.79	34700	174000	40300	12919	0.02	0.34
70	40	150	14.14	79100	219000	66100	30778	0.06	0.29
130	60	250	33.00	103000	318000	97900	35690	0.09	0.44
150	70	290	37.71	79000	388000	110000	24428	0.07	0.62
170	100	370	33.00	170000	403000	134000	65334	0.10	0.30
220	120	460	47.14	206000	476000	150000	81423	0.11	0.27
250	140	530	51.85	166000	490000	164000	56617	0.09	0.47
250	120	490	61.28	180000	485000	156000	66176	0.09	0.36
250	105	460	68.35	155000	518000	151000	56323	0.08	0.38

Table A-18 Anisotropic Material Properties for Gradation V3 at Optimum Moisture Content and with 2 Percent Stabilizer

σ_1 (kPa)	σ_3 (kPa)	I (kPa)	τ_{oct} (kPa)	E_x (kPa)	E_y (kPa)	G_{xy} (kPa)	G_{xx} (kPa)	ν_{xy}	ν_{xx}
40	25	90	7.07	733489	1374930	422259	240011	0.24	0.53
50	25	100	11.79	592193	1222316	468750	197372	0.05	0.50
70	40	150	14.14	952945	1521807	599042	361921	0.16	0.32
130	60	250	33.00	978342	1828911	648508	372954	0.13	0.31
150	70	290	37.71	908589	1937410	748503	317822	0.08	0.43
170	100	370	33.00	1161810	2021459	790306	463954	0.10	0.25

Table A-19 Anisotropic Material Properties for Gradation V4 at Optimum Moisture Content and with 2 Percent Stabilizer

σ_1 (kPa)	σ_3 (kPa)	I (kPa)	τ_{oct} (kPa)	E_x (kPa)	E_y (kPa)	G_{xy} (kPa)	G_{xx} (kPa)	ν_{xy}	ν_{xx}
130	60	250	33.00	832274	2277659	709891	288589	0.16	0.44
170	100	370	33.00	1127521	2630655	899820	427490	0.09	0.32
220	120	460	47.14	1222085	2422041	933610	508908	0.06	0.20
250	140	530	51.85	1351765	2625103	953390	558421	0.10	0.21

Table A-20 Anisotropic Material Properties for Gradation V1 at Wet of Optimum Moisture State and with 2 Percent Stabilizer

σ_1 (kPa)	σ_3 (kPa)	I (kPa)	τ_{oct} (kPa)	E_x (kPa)	E_y (kPa)	G_{xy} (kPa)	G_{xx} (kPa)	ν_{xy}	ν_{xx}
50	25	100	11.79	134192	374232	107759	53336	0.18	0.26
70	40	150	14.14	201945	372949	138122	103562	0.09	-0.03
130	60	250	33.00	260296	722902	183824	99854	0.15	0.30
150	70	290	37.71	334493	935565	266430	127229	0.14	0.31
170	100	370	33.00	363407	835339	281955	170735	0.12	0.06
220	120	460	47.14	506031	883396	319149	303969	0.04	-0.17
250	120	490	61.28	640464	1045789	362903	207432	0.09	0.54
250	105	460	68.35	552658	1132342	371287	320014	0.05	-0.14

Table A-21 Anisotropic Material Properties for Gradation V2 at Wet of Optimum Moisture State and with 2 Percent Stabilizer

σ_1 (kPa)	σ_3 (kPa)	I (kPa)	τ_{oct} (kPa)	E_x (kPa)	E_y (kPa)	G_{xy} (kPa)	G_{xx} (kPa)	ν_{xy}	ν_{xx}
50	25	100	11.79	110631	392056	89928	46511	0.13	0.19
70	40	150	14.14	154289	465560	140449	66743	0.18	0.16
130	60	250	33.00	283071	771990	202156	111018	0.13	0.27
150	70	290	37.71	402806	1003147	292398	149358	0.15	0.35
170	100	370	33.00	395383	892633	292398	158263	0.15	0.25
220	120	460	47.14	505901	1022787	328947	224207	0.10	0.13
250	140	530	51.85	559811	1176741	378788	239322	0.12	0.17
250	120	490	61.28	537579	1262602	374376	214663	0.13	0.25
250	105	460	68.35	571001	1280959	376884	238019	0.12	0.20

Table A-22 Anisotropic Material Properties for Gradation V3 at Wet of Optimum Moisture State and with 2 Percent Stabilizer

σ_1 (kPa)	σ_3 (kPa)	I (kPa)	τ_{oct} (kPa)	E_x (kPa)	E_y (kPa)	G_{xy} (kPa)	G_{xx} (kPa)	ν_{xy}	ν_{xx}
50	25	100	11.79	128190	340346	90253	57084	0.10	0.12
70	40	150	14.14	200182	441928	145914	86908	0.14	0.15
130	60	250	33.00	271537	616304	169300	115807	0.09	0.17
150	70	290	37.71	366454	799784	258176	140675	0.12	0.30
220	120	460	47.14	528035	941264	322812	235445	0.10	0.12
250	140	530	51.85	557005	1074495	357143	251539	0.09	0.11
250	120	490	61.28	578756	1125806	376884	248576	0.10	0.16
250	105	460	68.35	582115	1153167	365854	240849	0.11	0.21

Table A-23 Anisotropic Material Properties for Gradation V4 at Wet of Optimum Moisture State and with 2 Percent Stabilizer

σ_1 (kPa)	σ_3 (kPa)	I (kPa)	τ_{oct} (kPa)	E_x (kPa)	E_y (kPa)	G_{xy} (kPa)	G_{xx} (kPa)	ν_{xy}	ν_{xx}
50	25	100	11.79	172481	420253	117925	73349	0.10	0.18
70	40	150	14.14	262003	549253	178571	107589	0.15	0.22
130	60	250	33.00	359129	746230	212766	140382	0.11	0.28
150	70	290	37.71	476990	939285	302419	178353	0.14	0.34
220	120	460	47.14	609995	946891	343511	269901	0.11	0.13
250	140	530	51.85	718569	1003387	383959	372743	0.07	-0.04
250	120	490	61.28	741061	1120595	403226	335002	0.11	0.11
250	105	460	68.35	662417	1144670	383305	271932	0.12	0.22

APPENDIX B

TABLE OF MODULAR RATIOS

Table B-1 Modular Ratios for Gradation V1 at Optimum Moisture Content and with 0 Percent Stabilizer

σ_1 (kPa)	σ_3 (kPa)	I (kPa)	τ_{oct} (kPa)	E_x/E_y	G_{xy}/E_y	G_{xx}/G_{xy}
50	25	100	11.79	0.46	0.31	0.58
70	40	150	14.14	0.60	0.36	0.80
130	60	250	33.00	0.47	0.30	0.67
150	70	290	37.71	0.43	0.33	0.51
220	120	460	47.14	0.55	0.35	0.71
250	140	530	51.85	0.52	0.35	0.69
250	120	490	61.28	0.33	0.26	0.40
250	105	460	68.35	0.37	0.28	0.47

Table B-2 Modular Ratios for Gradation V2 at Optimum Moisture Content and with 0 Percent Stabilizer

σ_1 (kPa)	σ_3 (kPa)	I (kPa)	τ_{oct} (kPa)	E_x/E_y	G_{xy}/E_y	G_{xx}/G_{xy}
40	25	90	7.07	0.22	0.15	0.59
50	25	100	11.79	0.17	0.11	0.61
70	40	150	14.14	0.32	0.24	0.56
130	60	250	33.00	0.34	0.23	0.65
150	70	290	37.71	0.29	0.25	0.43
170	100	370	33.00	0.26	0.26	0.36
220	120	460	47.14	0.33	0.26	0.50
250	140	530	51.85	0.29	0.24	0.45
250	120	490	61.28	0.26	0.25	0.36
250	105	460	68.35	0.25	0.20	0.45

Table B-3 Modular Ratios for Gradation V3 at Optimum Moisture Content and with 0 Percent Stabilizer

σ_1 (kPa)	σ_3 (kPa)	I (kPa)	τ_{oct} (kPa)	E_x/E_y	G_{xy}/E_y	G_{xx}/G_{xy}
50	25	100	11.79	0.28	0.24	0.46
130	60	250	33.00	0.54	0.32	0.82
150	70	290	37.71	0.52	0.35	0.58
250	140	530	51.85	0.56	0.34	0.73
250	120	490	61.28	0.57	0.28	0.86
250	105	460	68.35	0.47	0.30	0.65

Table B-4 Modular Ratios for Gradation V4 at Optimum Moisture Content and with 0 Percent Stabilizer

σ_1 (kPa)	σ_3 (kPa)	I (kPa)	τ_{oct} (kPa)	E_x/E_y	G_{xy}/E_y	G_{xx}/G_{xy}
40	25	90	7.07	0.52	0.35	0.55
50	25	100	11.79	0.59	0.37	0.65
70	40	150	14.14	0.66	0.39	0.73
130	60	250	33.00	0.59	0.38	0.59
170	100	370	33.00	0.56	0.36	0.64
220	120	460	47.14	0.41	0.32	0.44
250	140	530	51.85	0.43	0.23	0.82
250	120	490	61.28	0.32	0.27	0.36

Table B-5 Modular Ratios for Gradation V1 at Wet of Optimum Moisture State and with 0 Percent Stabilizer

σ_1 (kPa)	σ_3 (kPa)	I (kPa)	τ_{oct} (kPa)	E_x/E_y	G_{xy}/E_y	G_{xx}/G_{xy}
40	25	90	7.07	0.16	0.11	0.57
50	25	100	11.79	0.17	0.16	0.43
70	40	150	14.14	0.39	0.31	0.66
130	60	250	33.00	0.28	0.22	0.50
150	70	290	37.71	0.36	0.29	0.47
170	100	370	33.00	0.47	0.33	0.60
220	120	460	47.14	0.55	0.35	0.74
250	140	530	51.85	0.55	0.34	0.74
250	120	490	61.28	0.31	0.21	0.56
250	105	460	68.35	0.41	0.28	0.64

Table B-6 Modular Ratios for Gradation V2 at Wet of Optimum Moisture State and with 0 Percent Stabilizer

σ_1 (kPa)	σ_3 (kPa)	I (kPa)	τ_{oct} (kPa)	E_x/E_y	G_{xy}/E_y	G_{xx}/G_{xy}
40	25	90	7.07	0.48	0.24	0.99
50	25	100	11.79	0.28	0.20	0.51
70	40	150	14.14	0.57	0.32	0.93
130	60	250	33.00	0.36	0.23	0.63
150	70	290	37.71	0.34	0.26	0.48
170	100	370	33.00	0.48	0.34	0.62
220	120	460	47.14	0.49	0.31	0.70
250	140	530	51.85	0.47	0.32	0.67
250	120	490	61.28	0.24	0.21	0.39
250	105	460	68.35	0.34	0.24	0.62

Table B-7 Modular Ratios for Gradation V3 at Wet of Optimum Moisture State and with 0 Percent Stabilizer

σ_1 (kPa)	σ_3 (kPa)	I (kPa)	τ_{oct} (kPa)	E_x/E_y	G_{xy}/E_y	G_{xx}/G_{xy}
50	25	100	11.79	0.17	0.15	0.43
70	40	150	14.14	0.38	0.27	0.75
130	60	250	33.00	0.21	0.16	0.51
150	70	290	37.71	0.22	0.19	0.44
170	100	370	33.00	0.36	0.28	0.61
220	120	460	47.14	0.35	0.24	0.72
250	140	530	51.85	0.37	0.26	0.72
250	120	490	61.28	0.13	0.13	0.35
250	105	460	68.35	0.12	0.12	0.34

Table B-8 Modular Ratios for Gradation V1 at Optimum Moisture Content and with 1 Percent Stabilizer

σ_1 (kPa)	σ_3 (kPa)	I (kPa)	τ_{oct} (kPa)	E_x/E_y	G_{xy}/E_y	G_{xx}/G_{xy}
40	25	90	7.07	0.45	0.23	0.85
50	25	100	11.79	0.42	0.23	0.30
70	40	150	14.14	0.59	0.35	0.76
130	60	250	33.00	0.56	0.33	0.80
150	70	290	37.71	0.50	0.33	0.59
170	100	370	33.00	0.54	0.35	0.65
220	120	460	47.14	0.65	0.37	0.87
250	140	530	51.85	0.60	0.36	0.83
250	120	490	61.28	0.38	0.26	0.50
250	105	460	68.35	0.42	0.29	0.59

Table B-9 Modular Ratios for Gradation V2 at Optimum Moisture Content and with 1 Percent Stabilizer

σ_1 (kPa)	σ_3 (kPa)	I (kPa)	τ_{oct} (kPa)	E_x/E_y	G_{xy}/E_y	G_{xx}/G_{xy}
50	25	100	11.79	0.93	0.44	1.02
70	40	150	14.14	1.32	0.51	1.12
130	60	250	33.00	0.89	0.39	0.81
150	70	290	37.71	1.23	0.50	1.08
170	100	370	33.00	1.28	0.50	1.17
220	120	460	47.14	1.14	0.47	1.17
250	140	530	51.85	1.02	0.48	1.03
250	120	490	61.28	0.61	0.35	0.54
250	105	460	68.35	0.71	0.38	0.64

Table B-10 Modular Ratios for Gradation V3 at Optimum Moisture Content and with 1 Percent Stabilizer

σ_1 (kPa)	σ_3 (kPa)	I (kPa)	τ_{oct} (kPa)	E_x/E_y	G_{xy}/E_y	G_{xx}/G_{xy}
40	25	90	7.07	0.60	0.34	0.73
50	25	100	11.79	0.31	0.25	0.45
70	40	150	14.14	0.48	0.33	0.58
130	60	250	33.00	0.52	0.35	0.64
150	70	290	37.71	0.58	0.36	0.70
170	100	370	33.00	0.57	0.37	0.66
220	120	460	47.14	0.54	0.37	0.63
250	140	530	51.85	0.42	0.33	0.50
250	120	490	61.28	0.31	0.29	0.32
250	105	460	68.35	0.44	0.31	0.50

Table B-11 Modular Ratios for Gradation V4 at Optimum Moisture Content and with 1 Percent Stabilizer

σ_1 (kPa)	σ_3 (kPa)	I (kPa)	τ_{oct} (kPa)	E_x/E_y	G_{xy}/E_y	G_{xx}/G_{xy}
50	25	100	11.79	0.20	0.39	0.14
70	40	150	14.14	1.00	0.45	1.04
130	60	250	33.00	0.85	0.41	0.77
150	70	290	37.71	0.85	0.49	0.67
170	100	370	33.00	0.65	0.42	0.57
220	120	460	47.14	0.68	0.43	0.72
250	140	530	51.85	0.62	0.40	0.73
250	120	490	61.28	0.90	0.44	1.11
250	105	460	68.35	1.07	0.45	1.17

Table B-12 Modular Ratios for Gradation V1 at Wet of Optimum Moisture State and with 1 Percent Stabilizer

σ_1 (kPa)	σ_3 (kPa)	I (kPa)	τ_{oct} (kPa)	E_x/E_y	G_{xy}/E_y	G_{xx}/G_{xy}
40	25	90	7.07	0.30	0.25	0.53
50	25	100	11.79	0.27	0.23	0.51
70	40	150	14.14	0.29	0.24	0.43
130	60	250	33.00	0.34	0.23	0.51
150	70	290	37.71	0.41	0.29	0.51
170	100	370	33.00	0.44	0.33	0.54
220	120	460	47.14	0.48	0.31	0.67
250	140	530	51.85	0.49	0.32	0.68
250	120	490	61.28	0.44	0.30	0.59
250	105	460	68.35	0.40	0.28	0.55

Table B-13 Modular Ratios for Gradation V2 at Wet of Optimum Moisture State and with 1 Percent Stabilizer

σ_1 (kPa)	σ_3 (kPa)	I (kPa)	τ_{oct} (kPa)	E_x/E_y	G_{xy}/E_y	G_{xx}/G_{xy}
70	40	150	14.14	0.32	0.25	0.42
130	60	250	33.00	0.30	0.22	0.50
150	70	290	37.71	0.37	0.29	0.47
170	100	370	33.00	0.40	0.31	0.54
220	120	460	47.14	0.42	0.29	0.64
250	140	530	51.85	0.40	0.30	0.60
250	120	490	61.28	0.36	0.28	0.54
250	105	460	68.35	0.36	0.27	0.55

Table B-14 Modular Ratios for Gradation V3 at Wet of Optimum Moisture State and with 1 Percent Stabilizer

σ_1 (kPa)	σ_3 (kPa)	I (kPa)	τ_{oct} (kPa)	E_x/E_y	G_{xy}/E_y	G_{xx}/G_{xy}
40	25	90	7.07	0.52	0.25	0.97
70	40	150	14.14	0.60	0.36	0.66
130	60	250	33.00	0.51	0.31	0.62
150	70	290	37.71	0.59	0.36	0.62
170	100	370	33.00	0.73	0.40	0.79
220	120	460	47.14	0.71	0.38	0.85
250	140	530	51.85	0.69	0.37	0.85
250	120	490	61.28	0.65	0.36	0.76
250	105	460	68.35	0.62	0.35	0.75

Table B-15 Modular Ratios for Gradation V4 at Wet of Optimum Moisture State and with 1 Percent Stabilizer

σ_1 (kPa)	σ_3 (kPa)	I (kPa)	τ_{oct} (kPa)	E_x/E_y	G_{xy}/E_y	G_{xx}/G_{xy}
50	25	100	11.79	0.20	0.34	0.16
70	40	150	14.14	1.48	0.50	1.40
130	60	250	33.00	0.91	0.44	0.93
150	70	290	37.71	1.34	0.52	1.48
170	100	370	33.00	0.73	0.43	0.67
220	120	460	47.14	1.01	0.45	1.36
250	140	530	51.85	0.57	0.39	0.59
250	120	490	61.28	0.76	0.43	0.82
250	105	460	68.35	0.85	0.43	0.94

Table B-16 Modular Ratios for Gradation V1 at Optimum Moisture Content and with 2 Percent Stabilizer

σ_1 (kPa)	σ_3 (kPa)	I (kPa)	τ_{oct} (kPa)	E_x/E_y	G_{xy}/E_y	G_{xx}/G_{xy}
40	25	90	7.07	0.64	0.33	0.79
50	25	100	11.79	0.26	0.26	0.34
70	40	150	14.14	0.70	0.38	0.96
130	60	250	33.00	0.59	0.35	0.81
150	70	290	37.71	0.62	0.38	0.71
220	120	460	47.14	0.72	0.39	0.96
250	140	530	51.85	0.70	0.40	0.90
250	120	490	61.28	0.39	0.28	0.47
250	105	460	68.35	0.55	0.35	0.68

Table B-17 Modular Ratios for Gradation V2 at Optimum Moisture Content and with 2 Percent Stabilizer

σ_1 (kPa)	σ_3 (kPa)	I (kPa)	τ_{oct} (kPa)	E_x/E_y	G_{xy}/E_y	G_{xx}/G_{xy}
40	25	90	7.07	0.36	0.27	0.63
50	25	100	11.79	0.20	0.23	0.32
70	40	150	14.14	0.36	0.30	0.47
130	60	250	33.00	0.32	0.31	0.36
150	70	290	37.71	0.20	0.28	0.22
170	100	370	33.00	0.42	0.33	0.49
220	120	460	47.14	0.43	0.32	0.54
250	140	530	51.85	0.34	0.33	0.35
250	120	490	61.28	0.37	0.32	0.42
250	105	460	68.35	0.30	0.29	0.37

Table B-18 Modular Ratios for Gradation V3 at Optimum Moisture Content and with 2 Percent Stabilizer

σ_1 (kPa)	σ_3 (kPa)	I (kPa)	τ_{oct} (kPa)	E_x/E_y	G_{xy}/E_y	G_{xx}/G_{xy}
40	25	90	7.07	0.53	0.31	0.57
50	25	100	11.79	0.48	0.38	0.42
70	40	150	14.14	0.63	0.39	0.60
130	60	250	33.00	0.53	0.35	0.58
150	70	290	37.71	0.47	0.39	0.42
170	100	370	33.00	0.57	0.39	0.59

Table B-19 Modular Ratios for Gradation V4 at Optimum Moisture Content and with 2 Percent Stabilizer

σ_1 (kPa)	σ_3 (kPa)	I (kPa)	τ_{oct} (kPa)	E_x/E_y	G_{xy}/E_y	G_{xx}/G_{xy}
130	60	250	33.00	0.37	0.31	0.41
170	100	370	33.00	0.43	0.34	0.48
220	120	460	47.14	0.50	0.39	0.55
250	140	530	51.85	0.51	0.36	0.59

Table B-20 Modular Ratios for Gradation V1 at Wet of Optimum Moisture State and with 2 Percent Stabilizer

σ_1 (kPa)	σ_3 (kPa)	I (kPa)	τ_{oct} (kPa)	E_x/E_y	G_{xy}/E_y	G_{xx}/G_{xy}
50	25	100	11.79	0.36	0.29	0.49
70	40	150	14.14	0.54	0.37	0.75
130	60	250	33.00	0.36	0.25	0.54
150	70	290	37.71	0.36	0.28	0.48
170	100	370	33.00	0.44	0.34	0.61
220	120	460	47.14	0.57	0.36	0.95
250	120	490	61.28	0.61	0.35	0.57
250	105	460	68.35	0.49	0.33	0.86

Table B-21 Modular Ratios for Gradation V2 at Wet of Optimum Moisture State and with 2 Percent Stabilizer

σ_1 (kPa)	σ_3 (kPa)	I (kPa)	τ_{oct} (kPa)	E_x/E_y	G_{xy}/E_y	G_{xx}/G_{xy}
50	25	100	11.79	0.28	0.23	0.52
70	40	150	14.14	0.33	0.30	0.48
130	60	250	33.00	0.37	0.26	0.55
150	70	290	37.71	0.40	0.29	0.51
170	100	370	33.00	0.44	0.33	0.54
220	120	460	47.14	0.49	0.32	0.68
250	140	530	51.85	0.48	0.32	0.63
250	120	490	61.28	0.43	0.30	0.57
250	105	460	68.35	0.45	0.29	0.63

Table B-22 Modular Ratios for Gradation V3 at Wet of Optimum Moisture State and with 2 Percent Stabilizer

σ_1 (kPa)	σ_3 (kPa)	I (kPa)	τ_{oct} (kPa)	E_x/E_y	G_{xy}/E_y	G_{xx}/G_{xy}
50	25	100	11.79	0.38	0.27	0.63
70	40	150	14.14	0.45	0.33	0.60
130	60	250	33.00	0.44	0.27	0.68
150	70	290	37.71	0.46	0.32	0.54
220	120	460	47.14	0.56	0.34	0.73
250	140	530	51.85	0.52	0.33	0.70
250	120	490	61.28	0.51	0.33	0.66
250	105	460	68.35	0.50	0.32	0.66

Table B-23 Modular Ratios for Gradation V4 at Wet of Optimum Moisture State and with 2 Percent Stabilizer

σ_1 (kPa)	σ_3 (kPa)	I (kPa)	τ_{oct} (kPa)	E_x/E_y	G_{xy}/E_y	G_{xx}/G_{xy}
50	25	100	11.79	0.41	0.28	0.62
70	40	150	14.14	0.48	0.33	0.60
130	60	250	33.00	0.48	0.29	0.66
150	70	290	37.71	0.51	0.32	0.59
220	120	460	47.14	0.64	0.36	0.79
250	140	530	51.85	0.72	0.38	0.97
250	120	490	61.28	0.66	0.36	0.83
250	105	460	68.35	0.58	0.33	0.71